ARTICLES
https://doi.org/10.1038/s42255-020-00271-w
nature metabolism

Check for updates

Stable human regulatory T cells switch to glycolysis following TNF receptor 2 costimulation

Sander de Kivit[1,2,3,9], Mark Mensink[1,2,3,9], Anna T. Hoekstra[4,9], Ilana Berlin[2,5], Rico J. E. Derks[6], Demi Both[3], Muhammad A. Aslam[3], Derk Amsen[7], Celia R. Berkers[4,8,10] ✉ and Jannie Borst[1,2,3,10] ✉

Following activation, conventional T (T_{conv}) cells undergo an mTOR-driven glycolytic switch. Regulatory T (T_{reg}) cells reportedly repress the mTOR pathway and avoid glycolysis. However, here we demonstrate that human thymus-derived T_{reg} (tT_{reg}) cells can become glycolytic in response to tumour necrosis factor receptor 2 (TNFR2) costimulation. This costimulus increases proliferation and induces a glycolytic switch in CD3-activated tT_{reg} cells, but not in T_{conv} cells. Glycolysis in CD3–TNFR2-activated tT_{reg} cells is driven by PI3-kinase–mTOR signalling and supports tT_{reg} cell identity and suppressive function. In contrast to glycolytic T_{conv} cells, glycolytic tT_{reg} cells do not show net lactate secretion and shuttle glucose-derived carbon into the tricarboxylic acid cycle. Ex vivo characterization of blood-derived TNFR2^{hi}CD4^{+}CD25^{hi}CD127^{lo} effector T cells, which were FOXP3^{+}IKZF2^{+}, revealed an increase in glucose consumption and intracellular lactate levels, thus identifying them as glycolytic tT_{reg} cells. Our study links TNFR2 costimulation in human tT_{reg} cells to metabolic remodelling, providing an additional avenue for drug targeting.

Among CD4^{+} T_{reg} cells, tTreg cells develop from T-cell precursors, recognize self-antigens and protect against autoimmunity[1]. Peripherally induced T_{reg} (pT_{reg}) cells, however, arise from mature T_{conv} cells that respond to foreign antigens and exert negative feedback on such responses[2]. The transcription factor forkhead box P3 (FOXP3) dictates T_{reg} differentiation fate[3,4]. In tT_{reg} cells, FOXP3 expression is stable, whereas pT_{reg} cells can lose FOXP3 expression and convert back to T_{conv} cells[5]. T_{reg} cells are used therapeutically against transplant rejection, graft-versus-host disease and autoimmunity[6,7]. For therapy, stable tT_{reg} cells must be used, since pT_{reg} cells may convert to T_{conv} cells and exacerbate, rather than attenuate, disease[6–8].

Selective (antibody) drug-based manipulation of T_{reg} cells is attractive in cancer, autoimmunity and transplant rejection[9,10]. Targeting via specific membrane receptors seems complicated, since T_{reg} and T_{conv} cells have many of these in common. However, downstream of the same receptor, the two cell types may use distinct signalling pathways. For example, T_{reg} cells reportedly attenuate the PI3-kinase (PI3K)–protein kinase B (Akt)–mammalian target of rapamycin (mTOR) pathway[11,12], which antagonizes FOXP3 expression[13]. Therefore, CD3–CD28-mediated T_{reg} cell expansion in the presence of the mTOR complex 1 (mTORC1) inhibitor rapamycin favours outgrowth of T_{reg} cells over contaminating T_{conv} cells[12]. Our recent data support the argument that signalling pathways in T_{conv} and T_{reg} cells are differentially 'wired', due to intrinsic differences in protein levels of key signal-transduction molecules[14].

T_{reg} and T_{conv} cells also appear to use distinct metabolic programmes. Once activated via the TCR–CD3 complex, with or without CD28 costimulation, T_{conv} cells become highly glycolytic[15]. In T_{conv} cells, CD3–CD28 signalling strongly activates the PI3K–Akt–mTOR pathway, which promotes glycolysis[16,17]. T_{reg} cells, in contrast, are thought to disfavour glycolysis[18–22]. Forced expression of FOXP3 in T_{conv} cells suppresses glycolysis and promotes fatty-acid oxidation (FAO)-fuelled oxidative phosphorylation (OXPHOS)[23,24]. Drivers of glycolysis reportedly antagonize FOXP3 expression and thereby compromise T_{reg} cell stability and function[19,25,26]. However, other studies suggest that T_{reg} cells require mTOR activity for in vivo function[27] and that human T_{reg} cells are highly glycolytic ex vivo[28] and require glycolysis to support FOXP3 expression and function[29]. The complexity of the cell populations studied may explain these discrepancies: tT_{reg} and pT_{reg} cells may have distinct metabolic programmes, and in vitro induced T_{reg} (iT_{reg}) cells may not faithfully represent pT_{reg} cells. Furthermore, pT_{reg} cells may (partly) convert back to T_{conv} cells in the assays employed.

We here studied the metabolism of pure human tT_{reg} cells and considered that a glycolytic switch may be induced by specific costimulatory receptors. We compared responses to CD28 and tumour necrosis factor receptor 2 (TNFR2, also known as TNFRSF1B or CD120b) costimulation in tT_{reg} and T_{conv} cells. TNFR2 was previously shown to be important for T_{reg} cell responses and protection against autoimmunity in humans and mice[30,31], and is considered a clinical target for selective T_{reg} expansion or inhibition in transplant rejection, autoimmunity or cancer[9,10]. We here report that CD3-activated tT_{reg} cells selectively respond to TNFR2 costimulation by proliferation and a PI3K–mTOR-driven glycolytic switch that is important for tT_{reg} cell identity and function. We also identify unique elements of the glycolytic programme in tT_{reg} cells and validate our findings in tT_{reg} cells directly isolated from human blood.

[1]Department of Immunohematology and Blood Transfusion, Leiden University Medical Center, Leiden, the Netherlands. [2]Oncode Institute, Leiden University Medical Center, Leiden, the Netherlands. [3]Division of Tumor Biology & Immunology, The Netherlands Cancer Institute, Amsterdam, the Netherlands. [4]Biomolecular Mass Spectrometry and Proteomics, Bijvoet Center for Biomolecular Research, Utrecht University, Utrecht, the Netherlands. [5]Department of Cell and Chemical Biology, Leiden University Medical Center, Leiden, the Netherlands. [6]Center for Proteomics and Metabolomics, Leiden University Medical Center, Leiden, the Netherlands. [7]Department of Hematopoiesis, Sanquin Research and Landsteiner Laboratory, Amsterdam, the Netherlands. [8]Department of Biomolecular Health Sciences, Faculty of Veterinary Medicine, Utrecht University, Utrecht, the Netherlands. [9]These authors contributed equally: Sander de Kivit, Mark Mensink, Anna T. Hoekstra. [10]These authors jointly supervised this work: Celia R. Berkers, Jannie Borst. ✉e-mail: c.r.berkers@uu.nl; j.g.borst@lumc.nl

Results

A new strategy allows for stable human T_{reg} cell expansion in the absence of rapamycin. Human T_{reg} cells occur in low frequency in the blood and, therefore, expansion protocols are used for clinical application[32]. In such protocols, T_{reg} cells are sorted by flow cytometry and expanded in presence of the mTOR inhibitor rapamycin that selectively inhibits proliferation of contaminating T_{conv} cells[12]. However, since rapamycin affects many aspects of metabolism, these expansion protocols are not suitable to generate T_{reg} cells for metabolic studies. Also, such cultures may still be contaminated with pT_{reg} cells that can convert back to T_{conv} cells and confound data interpretation. We therefore employed a new method to purify stable human tT_{reg} cells, based on the marker glycoprotein A33 (GPA33)[33].

Among $CD4^+$ T cells, naive T_{conv} cells were purified by flow cytometry on the basis of a $CD25^{lo}CD127^{hi}CD45RA^+GPA33^{int}$, phenotype and naive tT_{reg} cells on the basis of a $CD25^{hi}CD127^{lo}CD45RA^+GPA33^{hi}$ phenotype (Extended Data Fig. 1a). Phenotypic analysis of these populations indicated that the naive tT_{reg} cells could be discriminated from T_{conv} cells as previously defined[34] by expression of FOXP3, IKZF2 (HELIOS) and CTLA4 (Extended Data Fig. 1b). Sorted T cells were activated with agonistic monoclonal antibodies against CD3 and CD28 and were expanded in the presence of interleukin-2 (IL-2) for 14 d. Prior to analysis or restimulation, T cells were cultured from day 14 to day 18 in fresh medium with only IL-2 (Extended Data Fig. 2a). Data from multiple donors indicated that T_{reg} cells reactivated with monoclonal antibodies against CD3 and CD28 uniquely expressed FOXP3, IKZF2 and high levels of CTLA4 (Extended Data Fig. 2b,c). Expanded T_{reg} cells suppressed both $CD4^+$ and $CD8^+$ T_{conv} cell proliferation in a conventional suppression assay, wherein the T cells were activated to proliferate with anti-CD3 monoclonal antibody (Extended Data Fig. 2d). These data indicate that this GPA33-based, rapamycin-free expansion protocol yields a functional and stable human T_{reg} cell population of high purity.

Global changes in T_{conv} and tT_{reg} cells on CD3–CD28-mediated activation. We examined the response of T_{conv} and tT_{reg} cells to activation via CD3 and CD28, as this efficiently brings about the glycolytic switch in T_{conv} cells[15,16]. For this purpose, the two different cell types were generated according to the described expansion protocol. On day 18, the cells were restimulated with anti-CD3–CD28 monoclonal antibodies, in the presence of IL-2. CD28 expression levels were similar on both cell types (Fig. 1a). The expanded cells did not divide, unless they were stimulated with agonist monoclonal antibodies (Fig. 1b), indicating that they had become quiescent after withdrawal of anti-CD3–CD28 monoclonal antibodies on day 14 of the expansion protocol. Although T_{conv} cells already proliferated in response to CD3 triggering only, tT_{reg} cells were largely reliant on CD28 costimulation to do so (Fig. 1b). These data show that, under these in vitro circumstances, tT_{reg} cells depend more on CD28 costimulation than T_{conv} cells do to proliferate, which is in line with earlier findings[35].

To gain insight into the metabolic programme engaged by T_{conv} and tT_{reg} cells on CD3–CD28-mediated activation, we performed unbiased transcriptomic and metabolomic analyses. Expanded T_{conv} and tT_{reg} cells were rested and restimulated for 24 h with anti-CD3–CD28 monoclonal antibodies or not. Gene-expression profiling revealed that both T_{conv} and tT_{reg} cells readily responded to CD3–CD28-mediated reactivation, as indicated globally by principal component analysis (PCA). For both T_{conv} and tT_{reg} cells, the messenger-RNA profiles of CD3–CD28-stimulated populations were distinct from those of the unstimulated populations (Fig. 1c). Indicative of the functional distinction between T_{conv} and tT_{reg} cells, the genes responding to CD3–CD28-stimulation in both cell populations showed only a partial overlap (Extended Data Fig. 3a). Metabolomic analysis identified 109 water-soluble metabolites, including metabolites in central-carbon, nucleotide, amino-acid, carnitine and redox metabolism. The metabolite profile in CD3–CD28-stimulated T_{conv} cells was distinct from that in the unstimulated populations (Fig. 1c). In tT_{reg} cells, in contrast, CD3–CD28-mediated reactivation induced negligible differences in metabolite levels, as indicated by PCA (Fig. 1c) and the representation of altered metabolites in a Venn diagram (Extended Data Fig. 3a). These data indicate that expanded T_{conv} and tT_{reg} cells respond to CD3–CD28-mediated reactivation by proliferation and changes in gene expression, but tT_{reg} cells do not change their metabolic programme like T_{conv} cells.

T_{conv} but not tT_{reg} cells become overtly glycolytic upon CD3–CD28-mediated activation. We next zoomed in on the glycolytic pathway. In T_{conv} cells, several glycolytic intermediates increased significantly in abundance after CD3–CD28-mediated activation, including hexose phosphate (HexP) (that is, glucose-6P and fructose-6P), glyceraldehyde-3-phosphate, dihydroxyacetone phosphate (DHAP) and lactate. In tT_{reg} cells, however, among glycolytic intermediates only DHAP levels were significantly increased (Fig. 1d and Extended Data Fig. 4). Assays with the fluorescent glucose analogue 6-NBDG revealed that glucose uptake was increased in both T_{conv} and tT_{reg} cells upon CD3–CD28-mediated activation. However, glucose uptake was significantly higher in T_{conv} cells than in tT_{reg} cells (Fig. 1e).

Glycolytic flux is predominantly controlled by the expression of two glycolytic enzymes, hexokinase (HK) and phosphofructokinase (PFK)[36]. *HK2* mRNA expression was significantly increased in T_{conv} cells, but not in tT_{reg} cells on CD3–CD28-mediated activation (Fig. 1f). A proteomics data set of expanded human T_{conv} and T_{reg} cells that we had generated earlier[14] confirmed selective upregulation of HK2 in T_{conv} cells at the protein level after CD3–CD28 stimulation (Fig. 1g). Isoforms of PFK were upregulated at the mRNA level in both activated T_{conv} and tT_{reg} cells, but not at the protein level (Extended Data Fig. 3b,c). CD3–CD28-mediated activation led to immediate acidification of the growth medium and increased lactate secretion by T_{conv} cells, whereas no such changes were detected for tT_{reg} cells (Fig. 3h, i). The combined data indicate that, upon CD3–CD28-mediated activation, T_{conv} cells overtly increase their glycolytic activity, but tT_{reg} cells do not, in agreement with earlier reports[18,37].

TNFR2 costimulation promotes proliferation and maintains identity of tT_{reg} cells. Many data suggest that TNFR2 costimulation is important for T_{reg} cells and for maintenance of self-tolerance in humans[9,10,38]. A protocol for therapeutic T_{reg} expansion has been suggested, making use of TNFR2-agonist monoclnal antibody[39]. In our hands, in vitro–expanded tT_{reg} cells, but not T_{conv} cells, strongly upregulated cell-surface expression of TNFR2 upon reactivation via CD3 (Fig. 2a). Upon CD3-mediated activation, tT_{reg} cells clearly responded to TNFR2 costimulation by increased proliferation, whereas T_{conv} cells did not (Fig. 2b). Thus, costimulation via CD28 and TNFR2 induced cell proliferation in tT_{reg} cells that were activated via CD3 (Figs. 1b and 2b). TNFR2 activation alone, in the absence of CD3 stimulation, did not induce cell proliferation (Extended Data Fig. 5a).

We next examined the effects of CD3-mediated activation and CD28 or TNFR2 costimulation on tT_{reg} cell identity. As compared with activation via CD3 alone, costimulation via TNFR2 significantly increased FOXP3, IKZF2 and cell-surface CD25 protein expression, while total CTLA4 protein expression was not affected (Fig. 2c,d). TNFR2 activation alone did not affect expression levels of FOXP3, IKZF2 or CTLA4 (Extended Data Fig. 5a). In T_{conv} cells, TNFR2 and CD28 costimulation did not alter FOXP3, IKZF2, CD25 or CTLA4 protein levels as compared with levels

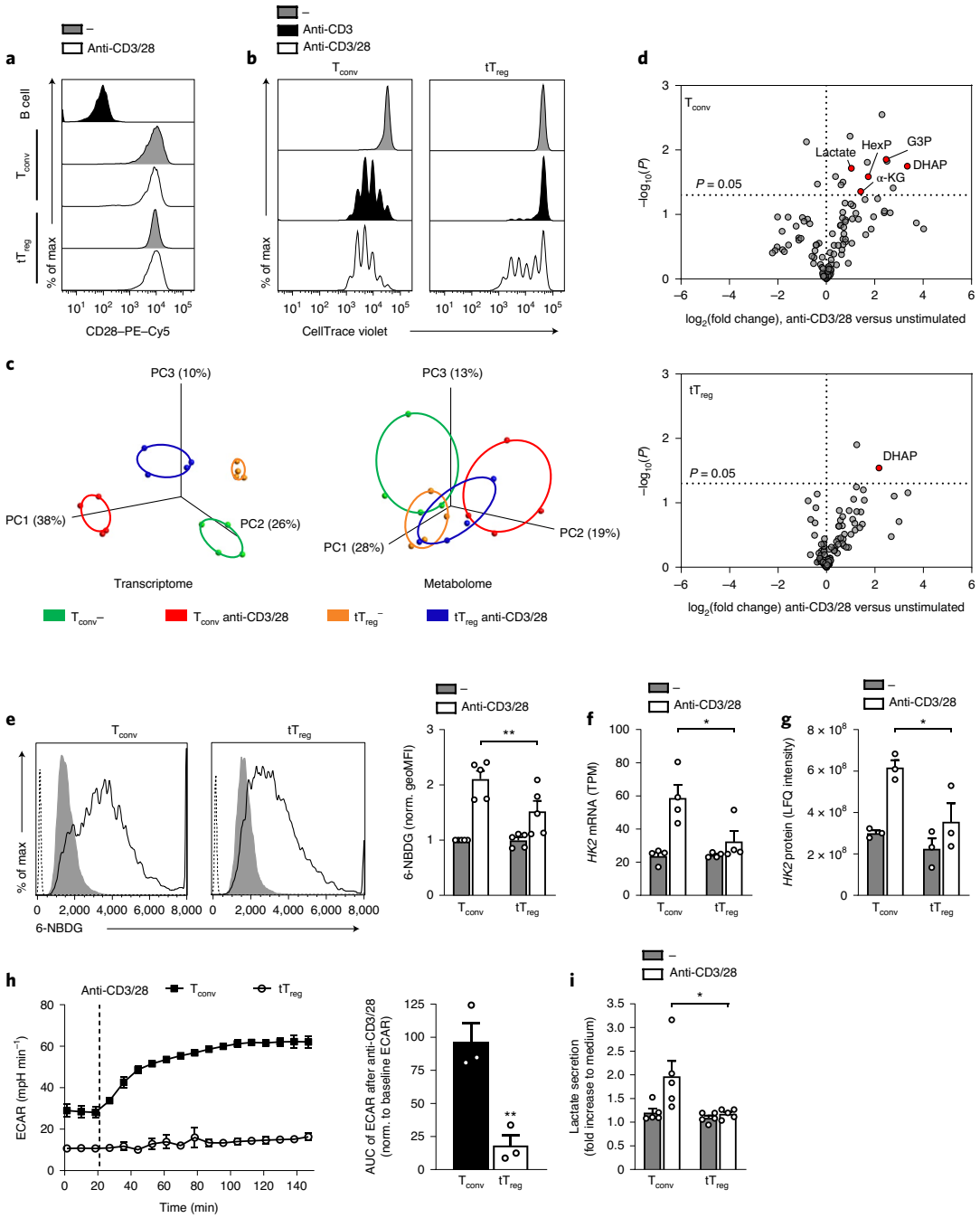

Fig. 1 | Analysis of glycolysis in T_{conv} and tT_{reg} cells after CD3–CD28-mediated activation. a, CD28 cell-surface expression, determined by flow cytometry, on the indicated cell types at 24 h after restimulation with monoclonal antibodies (mAbs) against CD3 and CD28 or unstimulated control (–) (representative of $n = 6$). B cells served as negative control. **b**, Flow-cytometric assessment of cell division according to CTV dilution, after stimulation as indicated for 96 h (representative of $n = 7$). **c**, PCA plots of transcriptomic (left, $n = 4$) and liquid chromatography–mass spectrometry (LC–MS)-based metabolomic (right, $n = 4$) analyses of expanded T_{conv} and tT_{reg} cells at 24 h after CD3–CD28-mediated restimulation or control (–). **d**, Volcano plots showing changes in the levels of 109 water-soluble metabolites in T_{conv} (top) and tT_{reg} (bottom) cells upon CD3–CD28-mediated restimulation ($n = 4$). Each circle represents one metabolite, with red colour denoting responding metabolites involved in glycolysis or the TCA cycle. Statistical analysis was done using an unpaired two-sided Student's *t*-test, and $P = 0.05$ is indicated by the dotted line. α-KG, α-ketoglutarate; G3P, glyceraldehyde-3-phosphate. **e**, Left, flow-cytometric analysis of glucose (6-NBDG) uptake at 24 h after restimulation as indicated. The dotted line indicates signal in absence of 6-NBDG. Right, quantification of 6-NBDG-uptake data based on geometric mean fluorescence intensity (geoMFI) normalized to unstimulated T_{conv} cells ($n = 5$), $^{**}P = 0.0067$. **f**, *HK2* mRNA levels derived from data set described in **c**, expressed in transcripts per million (TPM) ($n = 4$), $^{*}P = 0.026$. **g**, HK2 protein levels, expressed in label-free quantification (LFQ) intensity, as detected in an earlier proteome data set[14] ($n = 3$), $^{*}P = 0.0189$. **h**, Left, representative real-time measurement of extracellular acidification rate (ECAR) in T_{conv} and tT_{reg} cell cultures after CD3–CD28-mediated restimulation. Right, quantification of area under the curve (AUC) normalized to the baseline ECAR ($n = 3$, paired two-sided Student's *t*-test, $^{**}P = 0.007$). **i**, Lactate secretion as measured by LC–MS in the culture medium, expressed as fold increase relative to levels in culture medium without cells ($n = 5$), $^{*}P = 0.0274$. **e**–**i**, Two-way analysis of variance (ANOVA) with Tukey's post hoc test was used for statistical analysis unless stated otherwise. Data are presented as mean ± s.e.m. *n* represents cells from individual donors, analysed in independent experiments (**a**–**i**).

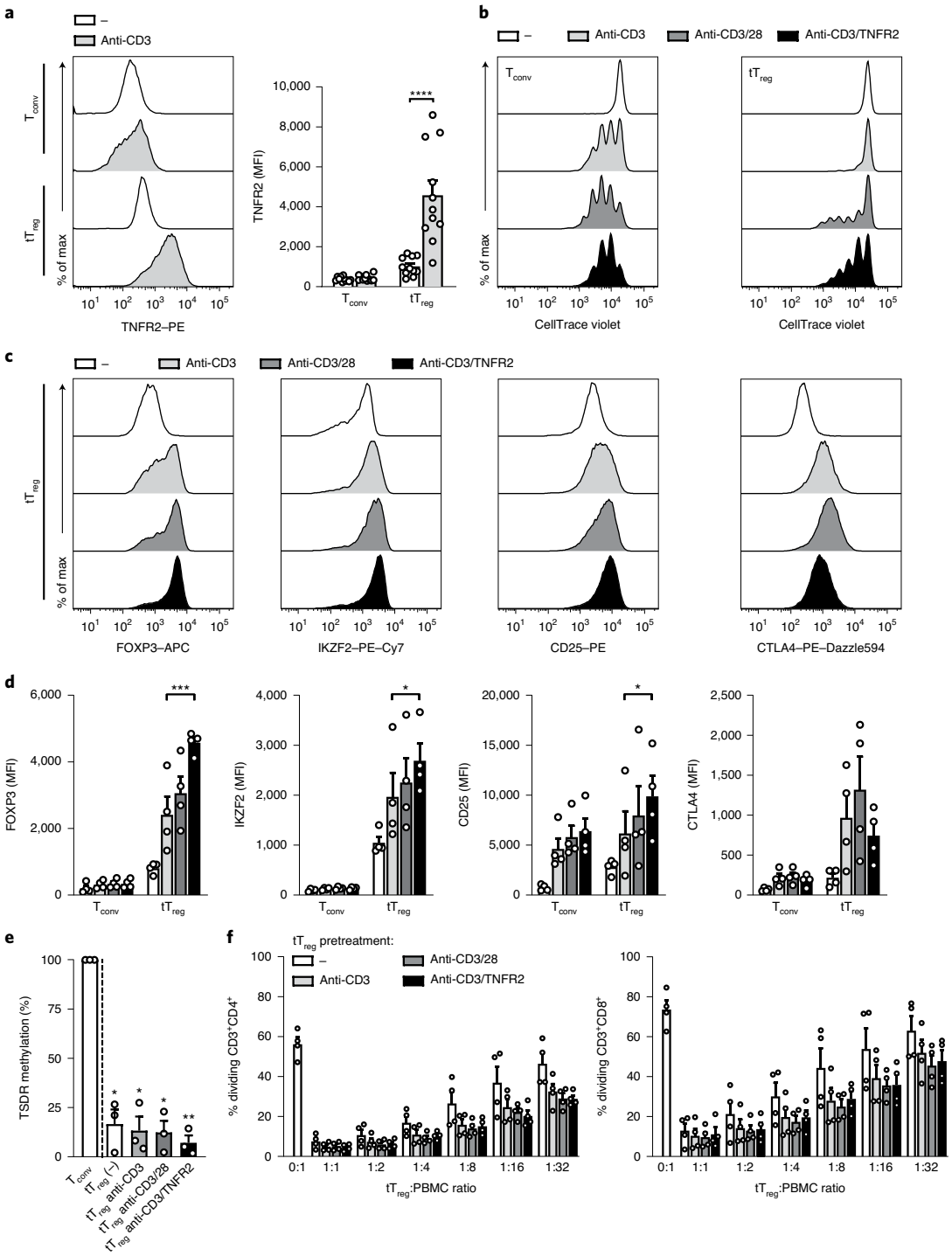

Fig. 2 | TNFR2 costimulation drives tT_{reg} cell proliferation while identity and suppressive function are maintained. a, Left, TNFR2 cell-surface expression, determined by flow cytometry, on T_{conv} and tT_{reg} cells at 24 h after restimulation with anti-CD3–CD28 mAbs or control (–). Right, quantification based on the MFI ($n = 11$), $^{****}P = 4.34 \times 10^{-5}$. **b**, Flow-cytometric assessment of T_{conv} and tT_{reg} cell division by CTV dilution at 96 h after restimulation as indicated (representative of $n = 7$). **c**, Flow-cytometric analysis of FOXP3, IKZF2, cell-surface CD25 and total CTLA4 protein expression in tT_{reg} cells at 24 h after restimulation as indicated (representative of $n = 4$). **d**, Quantification of flow cytometric data by MFI, including protein expression in Tconv cells from the same donors ($n = 4$), $^{***}P = 0.0006$ for FOXP3, $^{*}P = 0.0381$ and 0.013 for IKZF2 and CD25, respectively. Figure key in **c also applies to d**. **e**, Analysis of the methylation status of *FOXP3* TSDR in tT_{reg} cells at 24 h after restimulation as indicated. T_{conv} cells served as positive control ($n = 3$, one-way repeated-measures ANOVA with Dunnett's post hoc test, $^{*}P = 0.0173$, 0.0149, 0.0103 for tT_{reg} (–), tT_{reg} anti-CD3 and tT_{reg} anti-CD3/28 versus T_{conv}, respectively, and $^{**}P = 0.0036$ for tT_{reg} anti-CD3/TNFR2 versus T_{conv}). **f**, Assessment of suppressive capacity of tT_{reg} cells, prestimulated for 24 h as indicated and next cocultured for 96 h with CellTrace-Violet-labelled peripheral blood mononuclear cells (PBMCs) at different ratios, in the presence of agonistic monoclonal antibody against CD3. The percentage of dividing $CD4^+$ (left) or $CD8^+$ (right) responder T cells is displayed ($n = 4$). **a**,**d**–**f**, Two-way ANOVA with Tukey's post hoc test was used for statistical analysis unless stated otherwise. Data are presented as mean ± s.e.m. *n* represents cells from individual donors, analysed in independent experiments (**a**–**f**).

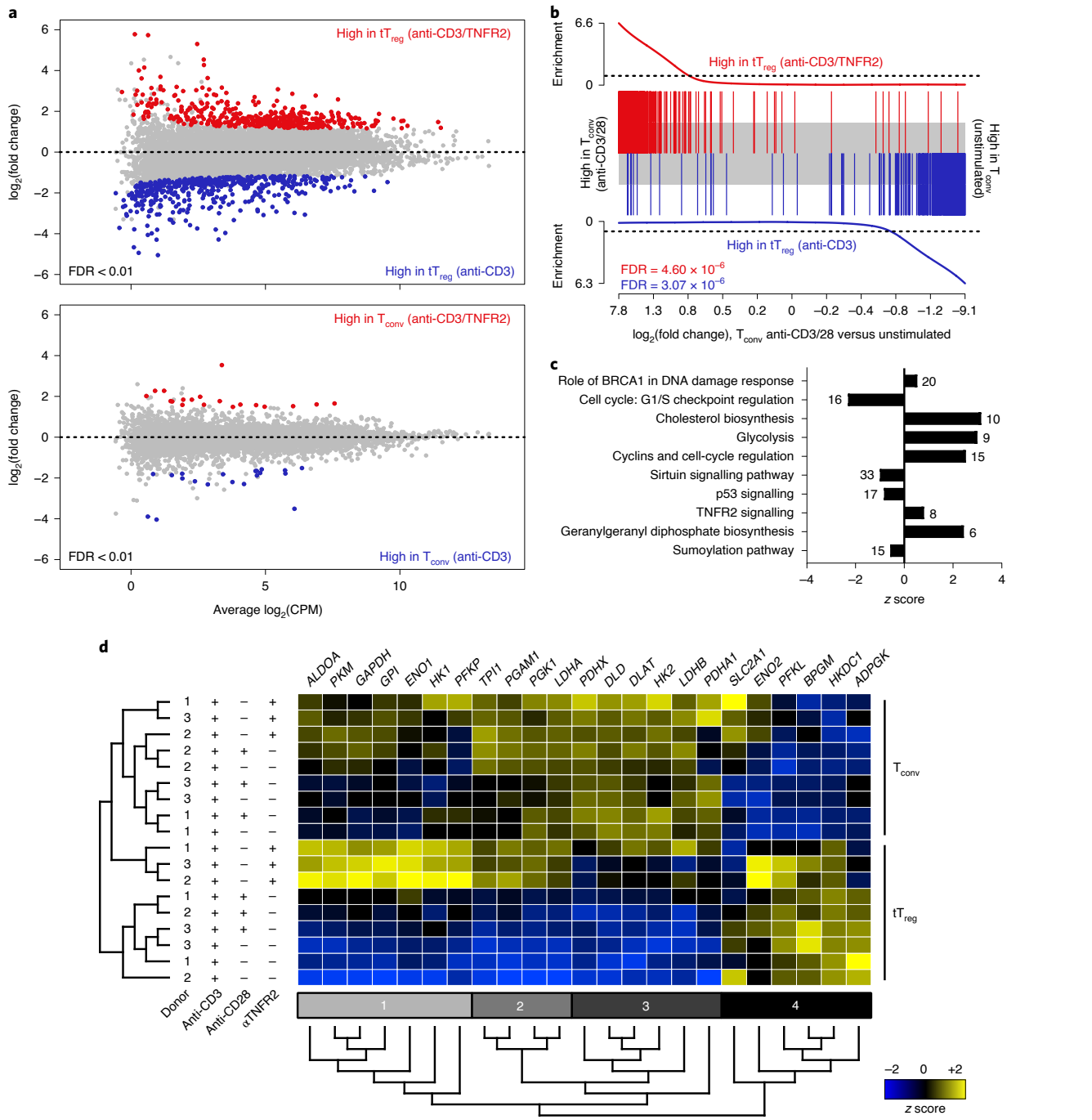

Fig. 3 | tT$_{reg}$ cells express glycolytic enzymes on TNFR2 costimulation. a, MA plots depicting results of comparative transcriptome analysis of tT$_{reg}$ (top) and T$_{conv}$ cells (bottom) that were activated via either CD3 or CD3 and TNFR2 for 24 h ($n = 3$, independent expansion cultures of distinct donors). Normalized read counts were analysed for log$_2$(read counts per million (CPM)) and differential expression by log$_2$(fold change) (false-discovery rate (FDR) < 0.01). Red and blue dots indicate transcripts with significant differential expression. **b**, Analysis of genes that were differentially expressed between CD3- and CD3–TNFR2-activated tT$_{reg}$ cells, with enrichment among high- or low-ranked genes. Ranking on the *x* axis was based on the log$_2$(fold change) in gene expression between CD3–CD28-activated and unstimulated T$_{conv}$ cells (grey bar), from the transcriptome data set described in Fig. 1. Genes that were differentially expressed between CD3- and CD3–TNFR2-activated tT$_{reg}$ cells were tested for enrichment (*y* axis) in the ranked list of genes expressed by T$_{conv}$ cells. Vertical bars correspond to genes that had higher expression levels in either CD3- (blue) or CD3–TNFR2-activated (red) tT$_{reg}$ cells, and are positioned according to the expression of those genes in T$_{conv}$ cells. Differential expression between CD3- and CD3–TNFR2-activated tT$_{reg}$ cells was determined by edgeR normalization and exact test (FDR < 0.01). Enrichment is indicated by graphs with scores higher than the dashed horizontal lines (FRY test). **c**, Evaluation of the 1,294 differentially expressed genes in tT$_{reg}$ cells upon CD3–TNFR2-mediated activation versus CD3-mediated activation alone (unpaired two-sided Student's *t*-test with Benjamini–Hochberg method; FDR < 0.05), showing the top ten significant pathways predicted to be up- or downregulated by IPA (right-tailed Fisher's exact test with Benjamini–Hochberg method; FDR < 0.05). Positive and negative *z* scores indicate up- and downregulated pathways, respectively. Numbers indicate quantity of differentially expressed genes involved in each pathway. **d**, Differential expression of indicated genes involved in glycolysis between T$_{conv}$ and tT$_{reg}$ cells that were stimulated for 24 h with agonistic mAbs against CD3, CD3–CD28 or CD3–TNFR2. *z* scores are colour-coded. Statistical evaluation was performed with an ANOVA with the Benjamini–Hochberg method; FDR < 0.05.

in CD3-stimulated cells (Fig. 2c,d). As *FOXP3* mRNA expression is epigenetically maintained by demethylation of the T_{reg}-specific demethylated region (TSDR) in the *FOXP3* gene[5], we analysed the methylation status of the TSDR in tT_{reg} cells that received CD28 or TNFR2 costimulation. As expected[5], the TSDR was highly demethylated in unstimulated tT_{reg} cells and methylated in T_{conv} cells (Fig. 2e). This epigenetic status of the TSDR in tT_{reg} cells was preserved when the cells were activated via CD3 alone or in conjunction with CD28 and TNFR2 costimulation (Fig. 2e).

These data indicate that costimulation via CD28 or TNFR2 does not destabilize tT_{reg} cells in terms of expression of their master regulator FOXP3. Accordingly, the suppressive capacity of tT_{reg} cells costimulated either via CD28 or TNFR2 was similar to the suppressive capacity of those stimulated via only CD3 (Fig. 2f). From these data, we conclude that TNFR2 delivers costimulatory signals for tT_{reg} cells, while preserving their identity and suppressive function.

TNFR2 costimulation induces expression of glycolysis-driving enzymes in tT_{reg} cells. We next performed transcriptomics to gain insights into the effects of TNFR2 costimulation on tT_{reg} and T_{conv} cells. This analysis showed in an unbiased manner that TNFR2 costimulation strongly affected gene expression in tT_{reg} cells, but not in T_{conv} cells (Fig. 3a and Extended Data Fig. 6a,b). Strikingly, gene-set enrichment analysis (GSEA) showed that the gene-expression profile of tT_{reg} cells that had been activated via CD3 and TNFR2 became more similar to the gene-expression profile of T_{conv} cells that had been activated via CD3 and CD28 (Fig. 3b). In contrast, the gene-expression profile of tT_{reg} cells that were stimulated via CD3 alone was enriched in the profile of unstimulated T_{conv} cells (Fig. 3b). These data suggest that tT_{reg} cells require TNFR2 costimulation to undergo the same type of transcriptional changes that T_{conv} cells undergo after activation via CD3 and CD28.

Ingenuity pathway analysis (IPA) was performed on the transcriptome data to examine which biological processes were affected in tT_{reg} cells by TNFR2 costimulation. IPA revealed that glycolysis is a significantly upregulated process in tT_{reg} cells upon TNFR2 costimulation (Fig. 3c). We zoomed into these data with the question of how CD3-activated tT_{reg} and T_{conv} cells alter the mRNA expression of glycolysis-pathway components after CD28 versus TNFR2 costimulation. Unsupervised hierarchical clustering (Fig. 3d) revealed that, after TNFR2 costimulation, tT_{reg} cells strongly upregulated specific molecules involved in glycolysis (cluster 1 and 2), of which some were already highly expressed in CD3–CD28-activated T_{conv} cells (cluster 2). Other molecules involved in glycolysis were differentially expressed in tT_{reg} and T_{conv} cells at the mRNA level, regardless of the stimulus (cluster 3 and 4). These data support the idea that TNFR2 costimulation induces a glycolytic switch in tT_{reg} cells.

tT_{reg} cells become glycolytic on TNFR2 costimulation, but do not show net lactate secretion. We next performed untargeted metabolomics to examine the metabolic changes in T_{conv} and tT_{reg} cells that occurred as a result of TNFR2 costimulation. In tT_{reg} cells, TNFR2 costimulation significantly altered the levels of 26 metabolites, as compared with CD3-mediated activation alone. These metabolites included intermediates of glycolysis, as well as the pentose-phosphate- and nucleotide-synthesis pathways. The main indicators of glycolytic flux fructose-1,6-bisphosphate (F-1,6-BP) and DHAP[36] were among the significantly changed metabolites in TNFR2-costimulated tT_{reg}, but not T_{conv}, cells, suggesting that glycolysis was upregulated by TNFR2 costimulation in tT_{reg} cells specifically. In T_{conv} cells, in contrast, TNFR2 costimulation significantly altered the levels of only seven metabolites (Fig. 4a and Extended Data Fig. 7). Interestingly, TNFR2 costimulation upregulated the same metabolites in tT_{reg} cells as did CD3 and CD28 stimulation in T_{conv} cells (Fig. 4b).

To confirm that tT_{reg} cells became glycolytic on TNFR2 costimulation, assays using the fluorescent glucose analogue 6-NBDG were performed. Indeed, TNFR2 costimulation significantly increased glucose-uptake activity in CD3-activated tT_{reg} cells (Fig. 4c). Glucose uptake in tT_{reg} cells after CD3–TNFR2-mediated activation reached levels similar to those in T_{conv} cells after CD3- or CD3- and CD28-mediated activation (Fig. 4c). TNFR2 stimulation alone, in the absence of CD3 stimulation, did not increase glucose-uptake activity by tT_{reg} cells (Extended Data Fig. 5b). In T_{conv} cells, increased glucose consumption occurs following translocation of the glucose transporter GLUT1 to the plasma membrane[16,40]. Activation of T_{conv} cells via CD3 resulted in GLUT1 translocation to the plasma membrane, whereas CD28 or TNFR2 costimulation had no additional effect (Fig. 4d). Interestingly, CD3-activated tT_{reg} cells showed only strong GLUT1 translocation to the plasma membrane upon TNFR2 costimulation, whereas CD28 costimulation had a more modest effect.

Strikingly, CD3–TNFR2-mediated activation did not result in immediate acidification of the growth medium (Fig. 4e) or net lactate release by tT_{reg} cells (Fig. 4f), whereas these events did occur in cultures of CD3-activated T_{conv} cells. Altogether, these results indicate that TNFR2 costimulation induces a glycolytic switch in CD3-activated tT_{reg} cells, as does CD3-mediated activation with or without CD28 costimulation in T_{conv} cells. Yet, tT_{reg} cells appear to employ a different metabolic programme downstream of glycolysis from that used by T_{conv} cells.

TNFR2-costimulated tT_{reg} cells complete the glycolytic pathway. To determine how tT_{reg} cells metabolize glucose as compared with how T_{conv} cells do this, we performed tracing experiments using [$^{13}C_6$]glucose (Fig. 5a). The data obtained clearly showed that TNFR2 costimulation activates the glycolytic pathway in CD3-activated tT_{reg} cells, since the levels of ^{13}C-labelled HexP, F-1,6-BP, DHAP, phosphoenolpyruvate (PEP), pyruvate and lactate were all significantly increased after TNFR2 costimulation (Fig. 5b). T_{conv} cells were already glycolytic after CD3 stimulation alone, and TNFR2 costimulation had no significant additional effects (Fig. 5b). Notably, upon TNFR2 costimulation, tT_{reg} cells built up higher intracellular levels of ^{13}C-labelled pyruvate ($P<0.01$) and similar levels of ^{13}C-labelled lactate as compared with those in CD3-activated T_{conv} cells (Fig. 5b). These results indicate that tT_{reg} cells can produce lactate from glucose and engage the complete glycolytic pathway upon TNFR2 costimulation, but that this does not result in net lactate secretion (Fig. 4e,f).

Both T_{conv} and tT_{reg} cells likely take up extracellular unlabelled (^{12}C) pyruvate from the cell-culture medium and convert this into lactate, as evidenced by the appearance of unlabelled pyruvate and lactate in these cells ($M+0$, Extended Data Fig. 8). However, the levels of unlabelled pyruvate and lactate do not increase on stimulation with CD3 or CD3 and TNFR2 in either cell type. These data suggest that TNFR2 costimulation in tT_{reg} cells promotes glycolytic flux, but not catabolism, of extracellular pyruvate.

TNFR2-costimulated tT_{reg} cells feed glucose-derived carbon into the TCA cycle. Both pyruvate and lactate[41] can be further metabolized in the tricarboxylic (TCA) cycle. In T_{conv} cells, stimulation via CD3 or CD3 and TNFR2 did not significantly increase the levels of labelled TCA-cycle intermediates, even though glycolytic flux was increased under these conditions (Fig. 5b,c). In contrast, the increase in glycolysis in TNFR2-costimulated tT_{reg} cells was accompanied by significantly higher levels of labelled TCA-cycle intermediates, compared with those accompanying no stimulation or CD3 stimulation alone. This suggests that in activated tT_{reg} cells, the increased glycolytic flux helps to sustain an increase in TCA-cycle flux. However, in T_{conv} cells, glycolysis appears to be uncoupled from the TCA cycle, and the increase in glycolytic flux instead results in the secretion

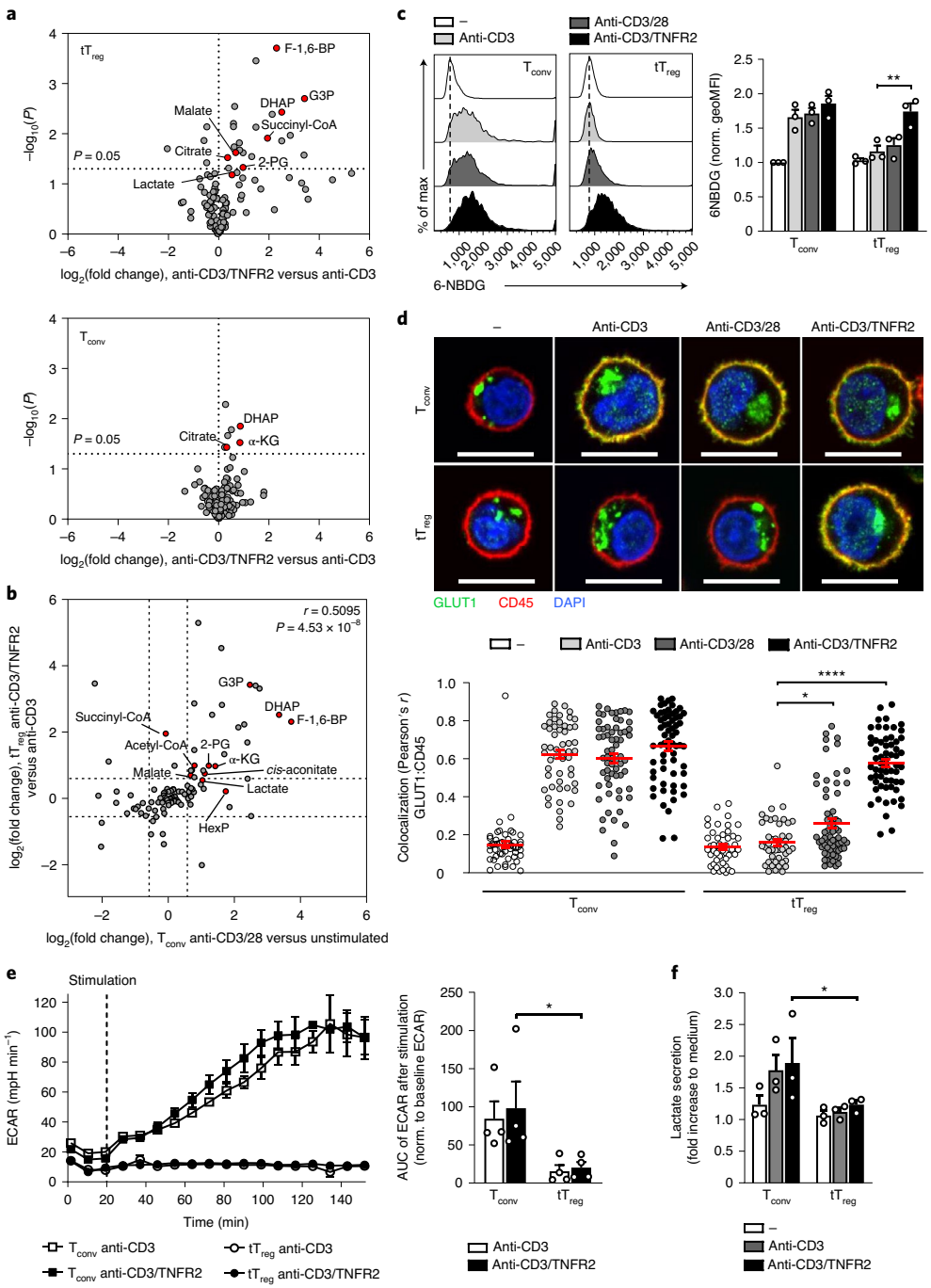

Fig. 4 | TNFR2 costimulation induces glycolysis in CD3-activated tT$_{reg}$ cells without increasing net lactate secretion. a, Volcano plots showing changes in levels of 135 water-soluble metabolites detected by LC–MS in expanded tT$_{reg}$ (top) or T$_{conv}$ cells (bottom), restimulated for 24 h via CD3 and TNFR2 versus CD3 alone ($n = 4$, independent expansion cultures of distinct donors). Statistical analysis was performed using an unpaired two-sided Student's *t*-test, with *p*-value of 0.05 indicated by the dotted horizontal line. Significant glycolysis and TCA-cycle intermediates are shown in red. 2-PG, 2-phosphoglycerate. **b**, Correlation plot comparing log$_2$(fold change) in metabolite levels in T$_{conv}$ cells upon restimulation via CD3 and CD28 (Fig. 1) with that in tT$_{reg}$ cells upon restimulation via CD3 and TNFR2. Dashed lines indicate log$_2$(fold change) of 0.58. Metabolites involved in glycolysis or the TCA cycle are shown in red ($r = 0.5095$; two-sided $P = 4.53 \times 10^{-8}$, by Pearson correlation). **c**, Left, flow cytometric assessment of 6-NBDG-uptake activity in T$_{conv}$ and tT$_{reg}$ cells restimulated for 24 h, as indicated. Dashed lines represent modal 6-NBDG uptake for unstimulated cells. Right, quantification of 6-NBDG-uptake data based on the geometric MFI, normalized to unstimulated T$_{conv}$ cells ($n = 3$), $^{**}P = 0.002$. **d**, Top, confocal-laser-scanning-microscopy-based assessment of subcellular GLUT1 localization in T$_{conv}$ and tT$_{reg}$ cells restimulated for 24 h as indicated. Images show cells stained for GLUT1 (green), plasma-membrane marker CD45 (red) and nuclear marker DAPI (blue). Scale bars, 10 µm. Bottom, quantification (two-sided Pearson's *r*) of GLUT1 colocalization with CD45 assessed on single cells ($n = 3$), $^{*}P = 0.0465$, $^{****}P < 1 \times 10^{-15}$. **e**, Left, representative real-time ECAR measurement in T$_{conv}$ and tT$_{reg}$ cell cultures following restimulation as indicated. Right, quantification of AUC, normalized to baseline ECAR ($n = 4$), $^{*}P = 0.0395$. **f**, Lactate secretion in culture medium of T$_{conv}$ and tT$_{reg}$ cells, as measured by LC–MS, expressed as fold increase relative to levels in medium without cells at 24 h following restimulation as indicated ($n = 3$), $^{*}P = 0.0256$. **c–f**, Two-way ANOVA with Tukey's post hoc test was used for statistical analysis. Data are presented as mean ± s.e.m. *n* represents cells from individual donors, analysed in independent experiments.

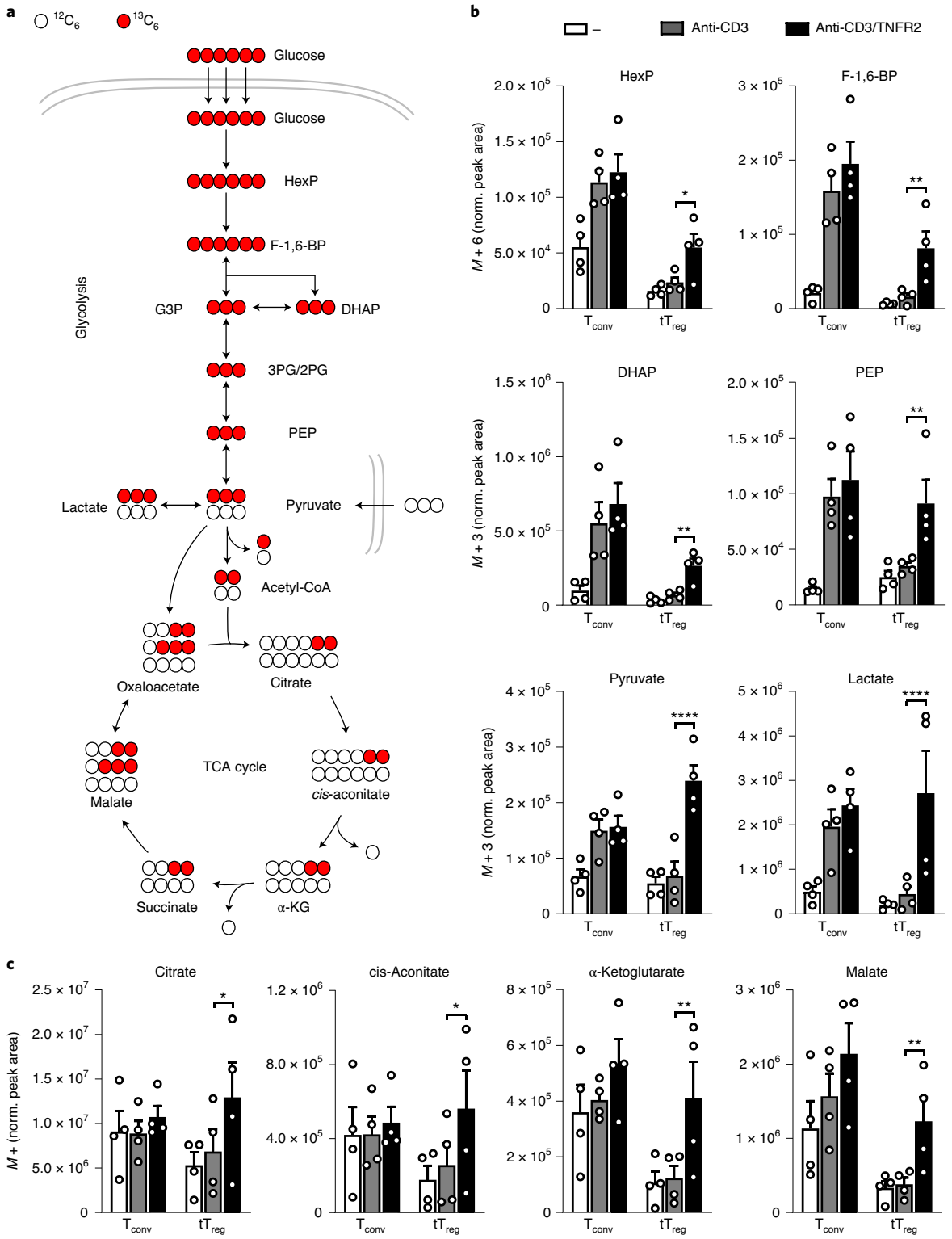

Fig. 5 | Tracing of [$^{13}C_6$]glucose shows increased flux through the glycolysis pathway and TCA cycle in tT_{reg} cells on TNFR2 costimulation. a, Schematic overview showing the tracing of [$^{13}C_6$]glucose into downstream intermediates of glycolysis and the TCA cycle. **b**, Analysis of the levels of ^{13}C-labelled intermediates of glycolysis in T_{conv} and tT_{reg} cells that were either unstimulated (–) or activated via CD3 or CD3 and TNFR2 for 24 h ($n = 4$), $^{*}P = 0.0138$ for [$^{13}C_6$]HexP, $^{**}P = 0.0045$, 0.005, and 0.0096 for [$^{13}C_6$]F-1,6-BP, [$^{13}C_3$]DHAP and [$^{13}C_3$]PEP, respectively, $^{****}P = 5.45 \times 10^{-7}$ and 7.29×10^{-6} for [$^{13}C_3$]pyruvate and [$^{13}C_3$]lactate, respectively, for tT_{reg} anti-CD3 versus tT_{reg} anti-CD3/TNFR2. **c**, Analysis of the levels of ^{13}C-labelled intermediates of the TCA cycle in T_{conv} and tT_{reg} cells that were either unstimulated (–) or activated via CD3 or CD3 and TNFR2 for 24 h ($n = 4$), $^{*}P = 0.0221$ and 0.0117 for [^{13}C]citrate and [^{13}C]*cis*-aconitate, respectively, $^{**}P = 0.0074$ and 0.0083 for [^{13}C]α-ketoglutarate and [^{13}C]malate, respectively, for tT_{reg} anti-CD3 versus tT_{reg} anti-CD3/TNFR2. Two-way ANOVA with Tukey's post hoc test was used for statistical analysis. Data are presented as mean ± s.e.m. *n* represents cells from independent expansion cultures of distinct donors (**b**,**c**).

of lactate (Fig. 4e,f). Of note, whereas the total levels of citrate and *cis*-aconitate did not differ significantly between activated T_{conv} and tT_{reg} cells, the levels of downstream α-ketoglutarate and malate were significantly lower in tT_{reg} cells compared with T_{conv} cells in all conditions tested (Extended Data Fig. 8). This result suggests that in tT_{reg} cells, part of the produced citrate leaves the TCA cycle for anabolic processes, instead of being converted to α-ketoglutarate. Altogether, these data indicate that tT_{reg} cells costimulated via TNFR2 increase their glycolytic activity, but use a different metabolic programme downstream of glycolysis than do T_{conv} cells.

Glycolysis induced by TNFR2 costimulation supports tT_{reg} cell function. To address the functional consequence of increased glycolysis in tT_{reg} cells following TNFR2 costimulation, restimulation experiments were performed in the presence of 2-deoxy-D-glucose (2-DG), a competitive inhibitor of hexokinase. TNFR2 costimulation significantly increased FOXP3 and IKZF2 expression by tT_{reg} cells (Fig. 2d). However, in the presence of 2-DG, FOXP3 expression was significantly reduced in tT_{reg} cells stimulated via CD3 and TNFR2, while IKZF2 expression remained unaffected (Fig. 6a, b). The expression of CTLA4 was reduced as well (Fig. 6a, b). The presence of 2-DG did not affect the viability of the cells (data not shown). In activated tT_{reg} cells costimulated via TNFR2 in the presence of 2-DG, reduced FOXP3 and CTLA4 expression was accompanied by reduced suppressive function (Fig. 6c). We therefore conclude that glycolysis supports the identity and suppressive function of CD3–TNFR2-stimulated tT_{reg} cells.

Costimulation via TNFR2 activates the mTOR pathway in tT_{reg} cells. The PI3K–Akt–mTOR pathway is known to be a key driver of glycolysis in T_{conv} cells following activation via CD3 and CD28 (ref. [15]). Since TNFR2 costimulation increased gene expression of glycolytic enzymes in tT_{reg} cells, we questioned whether TNFR2 costimulation activated the mTOR pathway. IPA predicted that the mTORC1 complex is an active upstream regulator of genes that were differentially expressed in TNFR2-costimulated tT_{reg} cells ($z=2.613$, $P=4.82\times10^{-4}$). GSEA confirmed that genes known to be upregulated via the PI3K–Akt–mTORC1 signalling pathway were enriched in CD3–TNFR2-stimulated tT_{reg} cells as compared with CD3 activation alone (Fig. 7a,b). Furthermore, expression of genes involved in nuclear factor-κB (NF-κB) signalling was enriched in CD3–TNFR2-activated tT_{reg} cells (Fig. 7c). These data suggest that PI3K–Akt–mTOR and NF-κB signalling are candidates for driving glycolysis in tT_{reg} cells upon TNFR2 costimulation.

We first addressed whether TNFR2 costimulation activates mTOR signalling. Flow-cytometric analysis of phosphorylation of mTOR (Ser2448) and its downstream target ribosomal protein S6 (Ser235/Ser236) showed that TNFR2 costimulation significantly enhanced mTOR signalling in tT_{reg} cells, as compared with CD3 activation alone (Fig. 7d,e). CD28 costimulation weakly activated mTOR and did not alter S6 phosphorylation in CD3-activated tT_{reg} cells. In T_{conv} cells, both mTOR and S6 were phosphorylated following CD28 or TNFR2 costimulation, although this was not significantly higher than following CD3 activation alone (Extended Data Fig. 9a,b). Similar results were observed when freshly isolated, CD3-activated tT_{reg} cells were costimulated via TNFR2, which was accompanied by increased glycolytic activity (Extended Data Fig. 9c–e). These data show that TNFR2 costimulation specifically activates the mTOR pathway in CD3-activated tT_{reg} cells.

To probe the mechanism by which TNFR2 costimulation drives mTOR signalling in tT_{reg} cells, we tested the impact of small-molecule inhibitors for PI3K (LY294002) and NF-κB-inducing kinase (NIK; NIK-SMI1) on the phosphorylation of mTOR and S6. Inhibition of PI3K, but not NIK, abrogated TNFR2-induced mTOR and S6 phosphorylation in CD3-activated tT_{reg} cells (Fig. 7f,g). As expected, blocking PI3K activity in CD3-activated T_{conv} cells decreased phosphorylation of mTOR and S6 (Extended Data Fig. 9f,g). The inhibitors did not affect cell viability (data not shown). Moreover, TNFR2 costimulation did not increase glucose consumption in tT_{reg} cells when mTOR or PI3K signalling was inhibited by rapamycin or LY294002, respectively, whereas NIK inhibition had no effect (Fig. 7h,i). These data indicate that TNFR2 costimulation induces a glycolytic switch in CD3-activated tT_{reg} cells by activation of mTORC1 signalling via PI3K.

TNFR2 expression level identifies glycolytic tT_{reg} cells in vivo. Finally, we aimed to address the connection between TNFR2 and glycolysis in tT_{reg} cells in vivo. For this purpose, we first discriminated $CD4^+CD25^{hi}CD127^{lo}$ putative T_{reg} cells in human blood on the basis of naive and effector phenotype and GPA33 levels (Fig. 8a, top). $CD45RA^+$ naive tT_{reg} cells were identified by high GPA33 expression (population 1), and $CD45RA^-$ effector phenotype cells could be subdivided into three populations with high, intermediate or low GPA33 expression. TNFR2 expression inversely correlated with GPA33 expression, with the highest TNFR2 expression on $CD45RA^-GPA33^{lo}$ effector cells (population 4) (Fig. 8a, bottom). Currently, there are no defining cell-surface markers for effector tT_{reg} cells, but we considered that a $TNFR2^{hi}$ phenotype identifies these cells. Within the $CD45RA^-GPA33^{lo}$ population, we sorted two subsets with either high or low TNFR2 expression (Fig. 8b, top). The $TNFR2^{hi}$ subset was uniformly $FOXP3^+$ and mainly $IKZF2^+$ (Fig. 8c, top, and 8d) and had uniformly high expression of CTLA4 (Fig. 8c, top, and 8e), indicating that this population was primarily composed of effector tT_{reg} cells. The $TNFR2^{lo}$ subset included $FOXP3^-$ T_{conv} cells, as well as $FOXP3^+IKZF2^-$ and $FOXP3^+IKZF2^+$ T_{reg} cells (Fig. 8c, top, and 8d). Within the $CD4^+CD25^{lo}CD127^{hi}GPA33^{lo}$ effector T_{conv} cell population, no TNFR2 expression was detected (Fig. 8b, bottom), and cells were predominantly $FOXP3^-$, $IKZF2^-$ and $CTLA4^-$ (Fig. 8c, bottom, and 8d,e).

To address whether $TNFR2^{hi}$ effector T_{reg} cells, as defined in Fig. 8c were glycolytic, we first assessed the expression levels of GLUT1 directly ex vivo. Effector T_{conv} and $TNFR2^{hi}$ effector T_{reg} cells had higher GLUT1 expression than the naive T_{conv} and T_{reg} cell populations, respectively (Fig. 8f). This was paralleled by increased glucose consumption, as reflected by increased uptake of 6-NBDG (Fig. 8g). These data suggested that in vivo, $TNFR2^{hi}$ effector T_{reg} cells exhibit increased glycolytic activity. To support this finding, we performed targeted metabolomics in ex-vivo-isolated $TNFR2^{hi}$ effector T_{reg} cells. Compared with naive tT_{reg} cells, $TNFR2^{hi}$ effector T_{reg} cells had increased levels of intracellular F-1,6-BP and lactate (Fig. 8h). We therefore conclude that a $TNFR2^{hi}$ phenotype identifies effector tT_{reg} cells in human blood with high glycolytic activity.

Discussion

Rapidly dividing cells switch their metabolic reliance from OXPHOS to aerobic glycolysis, which is less efficient in generating ATP, but glucose-derived carbon is used for the generation of nucleotides, amino acids and lipids that rapidly dividing cells require[42]. The glycolytic pathway and the connected TCA cycle also generate metabolites that support anabolic processes, or act as messengers or cofactors to direct cellular differentiation and function[43]. We here investigated whether well-defined, human thymus-derived T_{reg} cells can undergo a glycolytic switch when they are induced to proliferate.

T_{conv} cells switch to glycolysis upon TCR–CD3-mediated activation. CD28 is a costimulatory receptor that enforces the CD3 signal and promotes T-cell cycling, survival and glycolysis[16,44]. We found, in agreement with published data, that in vitro, human tT_{reg} cells do not efficiently proliferate upon CD3-mediated activation, but do so when additionally costimulated via CD28 (ref. [35]). Our data on glucose uptake, GLUT1 translocation, metabolomics and lactate secretion indicate that tT_{reg} cells do not become overtly glycolytic under these conditions, in contrast to T_{conv} cells. Transcriptome

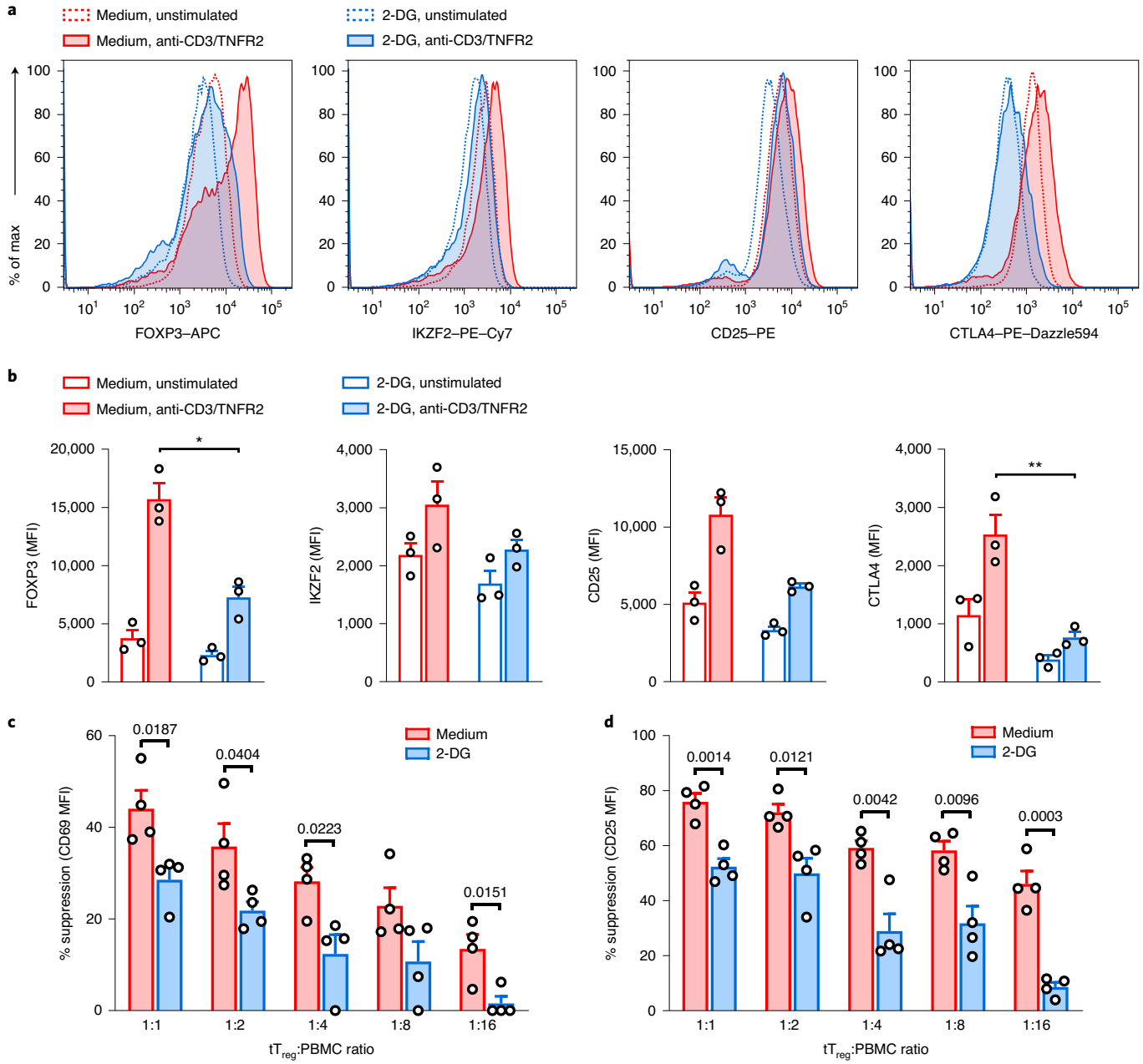

Fig. 6 | TNFR2-induced glycolysis maintains tT_{reg} cell identity and suppressive function. a, Flow-cytometric analysis of FOXP3, IKZF2, cell-surface CD25 and total CTLA4 protein expression in tT_{reg} cells at 24 h after restimulation with CD3 and TNFR2 or unstimulated controls with or without 2-DG (representative of $n=3$). **b**, Quantification of the data shown in **a** based on the MFI ($n=3$), $^{*}P=0.0199$, $^{**}P=0.0089$. Two-way ANOVA with Tukey's post hoc test was used for statistical analysis. **c**,**d**, Assessment of the suppressive capacity of tT_{reg} cells, prestimulated for 24 h via CD3 and TNFR2 with or without 2-DG, and subsequently cocultured with CTV-labelled PBMCs at different ratios for 24 h, in the absence of 2-DG and in the presence of agonistic mAb against CD3. The percentage suppression is calculated as detailed in the Methods, on the basis of the expression of CD69 (**c**) and CD25 (**d**) on the responder $CD3^{+}$ T cells ($n=4$). Unpaired two-sided Student's *t*-test was used for statistical analysis. Exact *P* values are indicated. Data are presented as mean ± s.e.m. *n* represents cells from individual donors, analysed in independent experiments (**a**–**d**).

analysis supported this conclusion, since expression of glycolytic enzymes was low in CD3-activated tT_{reg} cells and did not change upon CD28 costimulation. Hence, our analyses suggest that human tT_{reg} and T_{conv} cells use different metabolic programmes following CD3–CD28-mediated activation.

We found that, upon activation with anti-CD3 antibody, tT_{reg} cells responded to TNFR2 costimulation, whereas T_{conv} cells were inert to this costimulus. CD3-activated tT_{reg} cells switched to glycolysis upon TNFR2 costimulation, but not upon CD28 costimulation, while they proliferated following both. It is not known how these distinct costimulatory pathways are used by human tT_{reg} cells in vivo. CTLA4 serves to attenuate CD28 costimulation[45], suggesting that activated tT_{reg} cells that express high CTLA4 levels may avoid this costimulatory pathway. Our finding that high TNFR2 levels identify highly glycolytic effector phenotype tT_{reg} cells in human blood provided in vivo relevance for our findings and points to an important role of TNFR2 in human tT_{reg} cell physiology. TNFR2 signalling was shown by genetic studies in human and mice to be

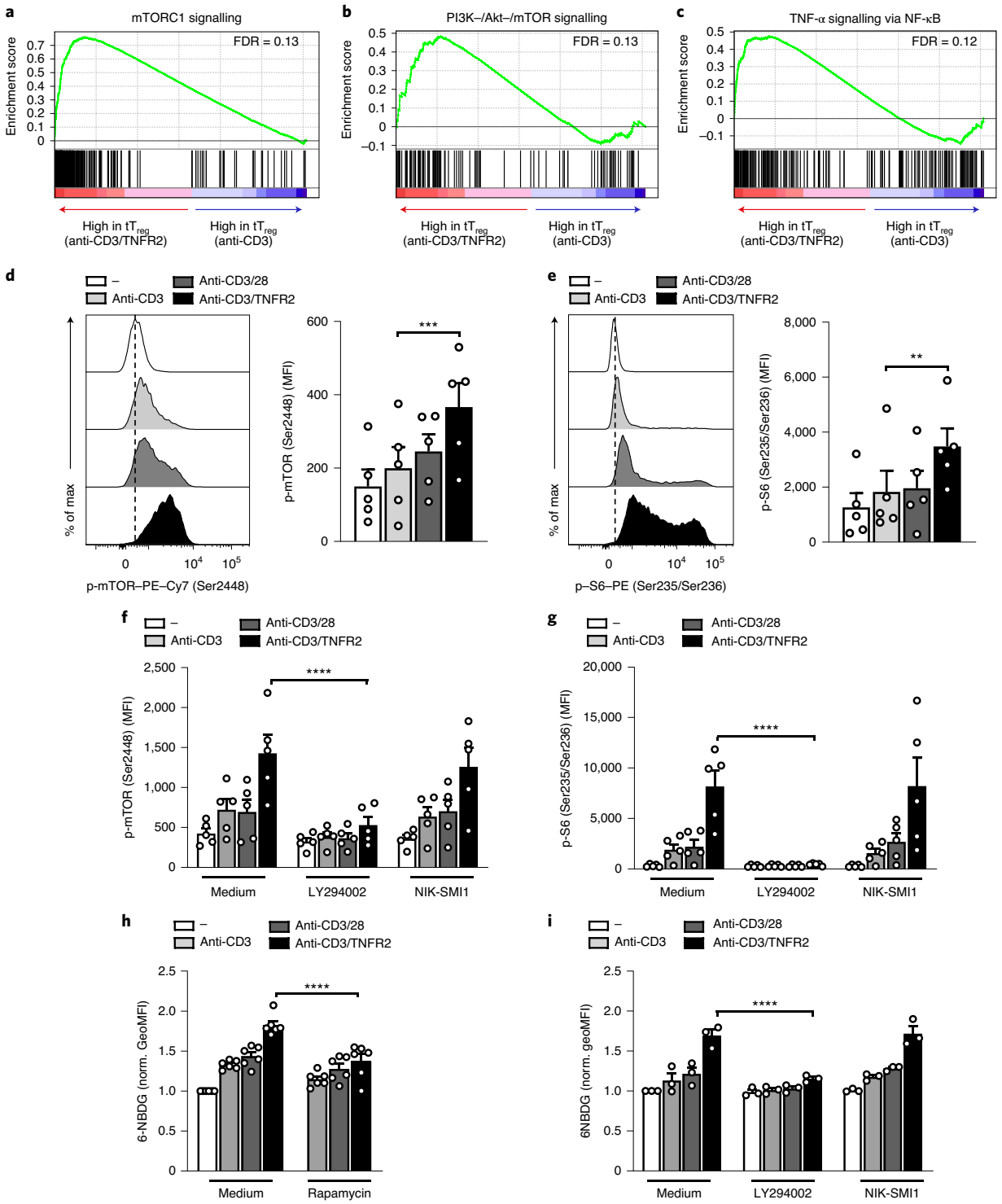

Fig. 7 | TNFR2 costimulation drives glycolysis in tT$_{reg}$ cells via PI3K and mTOR. a–c, GSEA of the hallmark gene sets mTORC1 signalling (**a**), PI3K–Akt–mTOR signalling (**b**) and TNF-α signalling via NF-κB (**c**) in tT$_{reg}$ cells activated via CD3–TNFR2 or CD3 alone from the transcriptome data set described in Fig. 3 ($n=3$ independent expansion cultures of distinct donors). **d**,**e**, Left, representative flow-cytometric analysis of phosphorylated mTOR (Ser2448) (**d**) and S6 (Ser235/Ser236) (**e**) levels in tT$_{reg}$ cells following restimulation for 24 h as indicated. Right, quantification based on the MFI ($n=5$), $^{***}P=0.0002$ for p-mTOR (Ser2448) and $^{**}P=0.0013$ for p-S6 (Ser235/Ser236). One-way repeated-measures ANOVA with Bonferroni's post hoc test was used for statistical analysis. **f**,**g**, Quantification of flow-cytometric analysis of phosphorylated mTOR (Ser2448) (**f**) or S6 (Ser235/Ser236) (**g**) levels in tT$_{reg}$ cells following restimulation for 24 h as indicated in presence or absence of selective inhibitors of PI3K (LY294002) or NIK (NIK-SMI1) in the culture medium ($n=5$), $^{****}P=1.43\times10^{-8}$ and 1.16×10^{-7} for phosphorylated mTOR and S6, respectively. **h**,**i**, Flow-cytometric assessment of 6-NBDG-uptake activity in tT$_{reg}$ cells that were restimulated for 24 h as indicated, in the presence or absence of selective inhibitors of mTOR (rapamycin) ($n=6$, $^{****}P=5.0\times10^{-5}$) (**h**), PI3K (LY294002) or NIK (NIK-SMI1) ($n=3$, $^{****}P=1.53\times10^{-5}$) (**i**). Data were analysed on the basis of the geometric MFI, normalized to that of unstimulated tT$_{reg}$ cells. **f**–**i**, Two-way ANOVA with Tukey's post hoc test was used for statistical analysis. Data are presented as mean ± s.e.m. *n* represents cells from individual donors, analysed in independent experiments (**d**–**i**).

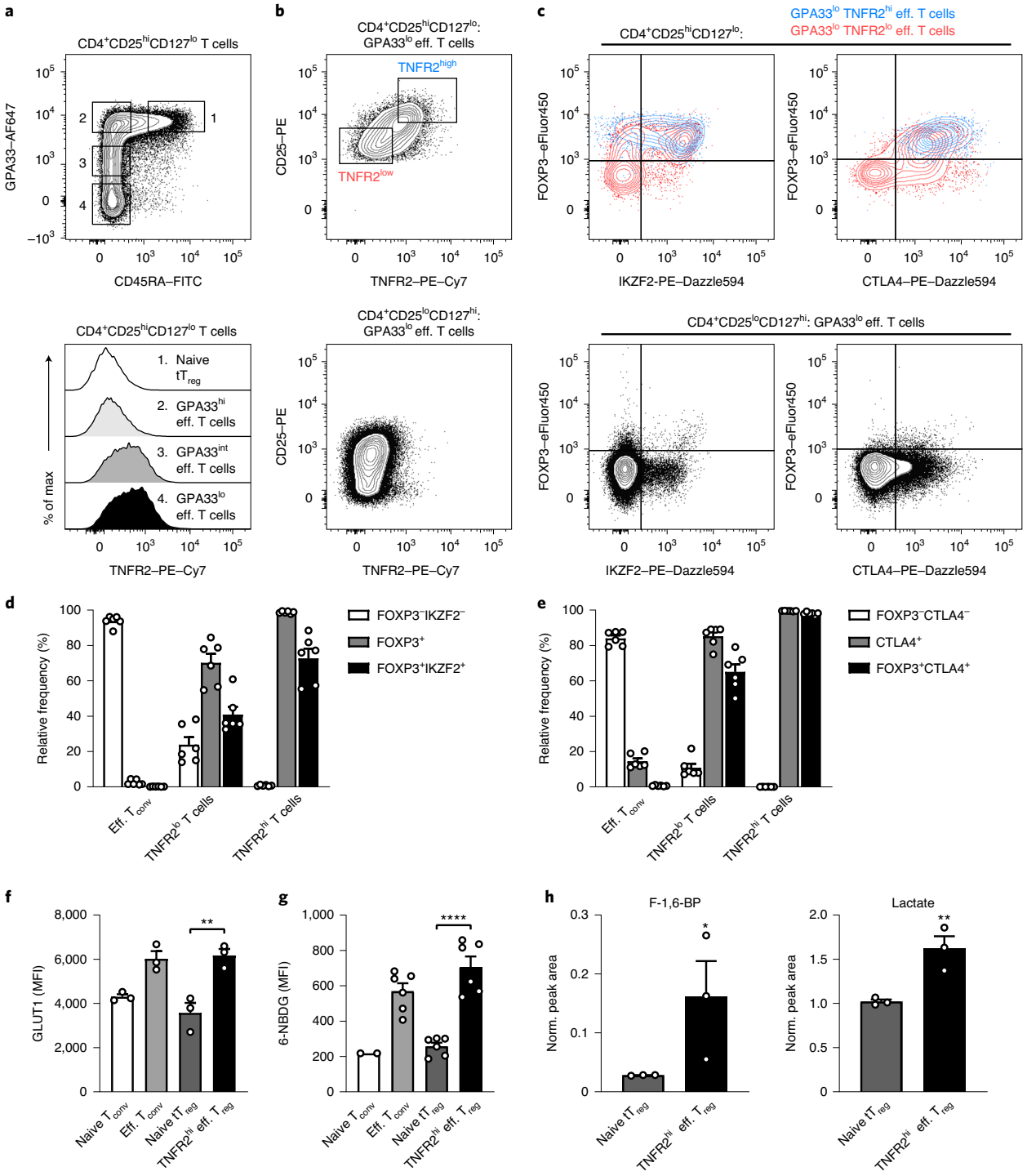

Fig. 8 | In vivo effector T_{reg} cells that express high levels of TNFR2 are primarily tT_{reg} cells and have increased glycolytic activity. a, Flow-cytometric analysis of CD4$^+$CD25^{hi}CD127^{lo} putative T_{reg} cells within human PBMCs. CD45RA and GPA33 markers were used to distinguish naive tT_{reg} cells (population 1) and three effector (eff.) cell populations (top). TNFR2 expression levels on these four populations are shown in the bottom panel (representative of $n=6$). **b**, Top, sorting strategy for the isolation of TNFR2^{hi} and TNFR2^{lo} cells from the CD45RA$^-$GPA33^{lo} putative effector T_{reg} cell population (population 4). Bottom, TNFR2 and CD25 expression on CD4$^+$CD25^{lo}CD127^{hi}CD45RA$^-$GPA33^{lo} effector T_{conv} cells (representative of $n=6$). **c**, Flow-cytometric analysis showing FOXP3, IKZF2 and total CTLA4 expression within the TNFR2^{hi} and TNFR2^{lo} subpopulations of the putative effector T_{reg} cell population (top) and on effector T_{conv} cells (bottom), as described in **b** (representative of $n=6$). **d**,**e**, Quantification of data shown in **c** ($n=6$). **f**, Evaluation of total GLUT1 levels in the indicated T_{conv} and T_{reg} cell populations, based on the MFI as analysed by flow cytometry ($n=3$), $^{**}P=0.0021$. **g**, Flow-cytometric assessment of 6-NBDG uptake in the indicated T_{conv} and T_{reg} cell populations, as analysed directly following cell sorting ($n=2$ for naive T_{conv} cells, $n=6$ for effector T_{conv}, naive tT_{reg} and TNFR2^{hi} effector T_{reg} cells), $^{****}P=3.25\times10^{-5}$. **h**, Analysis of the intracellular levels of F-1,6-BP and lactate as determined by targeted metabolomics in freshly isolated naive tTreg cells and TNFR2^{hi} effector T_{reg} cells ($n=3$ independent donors), $^{*}P=0.0283$, $^{**}P=0.0075$. **f**–**h**, An unpaired two-sided Student's t test was used for statistical analysis of naive tT_{reg} cells and TNFR2^{hi} effector T_{reg} cells. Data are presented as mean ± s.e.m. Sample size (n) represents cells from individual donors, analysed in independent experiments (**a**–**g**).

important for maintenance of self-tolerance[30,31]. In addition, TNFR2 was shown to be uniquely important for driving T_{reg} responses and is therefore proposed as a clinical target[9,10]. TNFR2, as opposed to TNFR1, preferentially responds to membrane-bound TNF rather than to soluble TNF[46]. Currently, the tissue context in which T_{reg} cells receive costimulatory input via TNFR2 is not known, except that membrane-bound TNF on T_{reg} cells themselves[47] and on tolerogenic monocyte-derived dendritic cells[48] can promote T_{reg} cell expansion. TNFR2 costimulation also drives T_{reg} expansion in vivo in mice[49]. Agonistic monoclonal antibody against TNFR2 has therefore been used to expand CD3-activated human T_{reg} cells in vitro[39].

In expansion protocols of human tT_{reg} cells intended for therapeutic purposes, rapamycin is included to avoid outgrowth of contaminating T_{conv} cells[11]. Recently, we identified the type I transmembrane molecule GPA33 as a novel surface marker expressed exclusively by naive tT_{reg} cells[14] that can be used for isolation of these cells from human peripheral blood[33]. GPA33 is an Ig superfamily member originally found predominantly on colon carcinoma cells[50], but its function in T cells is unknown. In the current study, we have used GPA33 in a new purification protocol for human tT_{reg} cells allowing in-depth metabolic analyses in these cells without confounding effects of rapamycin on their metabolism. The current literature data on human T_{reg} cell metabolism is confusing, because different (mixed) cell populations are studied. For example, freshly isolated human T_{reg} cells stimulated via CD3 and CD28 were found to rely on both glycolysis and fatty-acid oxidation[28]. In that study, T_{reg} cells partially lost their suppressive function and FOXP3 expression upon stimulation, which suggests presence of pT_{reg} cells in the test material. In in vitro–induced T_{reg} cells, in contrast, glycolysis supported FOXP3 expression after CD3–CD28-mediated activation[29]. We demonstrate that TNFR2 costimulation reinforces tT_{reg} cell identity by upregulation of FOXP3 and IKZF2 and find that glycolysis is required for this effect, as well as for the suppressive function of TNFR2-costimulated tT_{reg} cells. Interestingly, TNFR2-costimulated tT_{reg} cells relied on PI3K and mTOR to activate glycolysis, as do T_{conv} cells after CD3 and CD28 stimulation[16,40]. TNFR2 uses a very different signalling mechanism than CD3 and CD28 do, which is based on TRAF and ubiquitin signalling and activity of serine–threonine kinase, rather than tyrosine-kinase activity[38,41]. TNF receptor family members activate canonical and non-canonical NF-κB signalling via NIK, which is linked to cell survival[9,10,38]. We found no impact of NIK inhibition on the TNFR2-induced glycolytic switch in T_{reg} cells. Further study will need to point out how activation of PI3K–mTOR signalling is enabled in tT_{reg} cells by CD3–TNFR2-mediated activation.

We found that in glycolytic tT_{reg} cells, the fate of glucose-derived carbon was different than in glycolytic T_{conv} cells. TNFR2-costimulated tT_{reg} cells produced lactate from glucose, but did not show net lactate secretion. Lactate is actively shuttled in and out of cells by specific membrane transporters and can be used in the TCA cycle or other metabolic pathways. However, it can also act as an intracellular or extracellular signalling molecule and, among other activities, modulate immune-cell function by regulating gene expression[51]. In glycolytic tT_{reg} cells, the increase in glycolysis was coupled to an increased shuttling of glycolysis intermediates into the TCA cycle.

The TCA cycle also generates precursors for a number of biosynthetic pathways. Citrate can exit the mitochondria and can be converted to acetyl-CoA in the cytosol by ATP citrate lyase. Thereby, citrate serves as an important precursor for both fatty-acid synthesis and the mevalonate pathway that produces cholesterol[52,53]. Glycolytic tT_{reg} and T_{conv} cells had similar levels of citrate, but the levels of downstream TCA-cycle intermediates such as α-ketoglutarate and malate were significantly lower in tT_{reg} cells, suggesting that part of the produced citrate is indeed funnelled into anabolic processes. In murine T_{reg} cells, the mevalonate pathway was shown to be important in coordinating T_{reg} proliferation, suppressive capacity and lineage stability[54,55]. Moreover, mTORC1 was recently shown to be important for upregulation of mitochondrial metabolic pathways, including the TCA cycle[27], and to promote cholesterol synthesis via the mevalonate pathway in T_{reg} cells[55]. We propose that TNFR2 costimulation in tT_{reg} cells may support the mevalonate pathway by upregulating TCA-cycle activity. Our transcriptome analysis indeed suggests that TNFR2 costimulation supports cholesterol biosynthesis and geranylgeranyl diphosphate biosynthesis pathways in proliferating tT_{reg} cells, both of which require the mevalonate pathway.

In conclusion, our study identified a new role for TNFR2 costimulation in regulating glucose metabolism in human tT_{reg} cells. In addition, we provide evidence that tT_{reg} cells have metabolic adaptions downstream of glycolysis that may be related to tT_{reg}-cell functionality. Further understanding of the key signalling events and metabolic adaptions in tT_{reg} cells following TNFR2 activation may reveal unique targets to specifically modulate tT_{reg} cell function in transplant rejection, autoimmunity and cancer.

Methods

Cell isolation and flow cytometric sorting. Human materials were obtained in accordance with the Declaration of Helsinki and the Dutch rules with respect to the use of human materials from volunteer donors. Buffy coats from healthy anonymized male donors were obtained after their written informed consent, as approved by Sanquin's internal ethical board. Human PBMCs were isolated from buffy coats using Ficoll-Paque Plus density gradient centrifugation (GE Healthcare). Subsequently, total $CD4^+$ T cells were isolated by using CD4 magnetic MicroBeads (MACS, Miltenyi Biotec) according to the manufacturer's protocol. Alternatively, $CD4^+$ T cells were isolated directly from the buffy coat using the StraightFrom Buffy Coat CD4 MicroBead kit (Miltenyi Biotec). For sorting, T_{conv} and tT_{reg} cells were stained with combinations of CD4–PE–Cy7/CD4–BB700, CD127–BV421 (BioLegend), CD25–PE (BD Biosciences), CD45RA–FITC/CD45RA–APC–Cy7/CD45RA–BV650, GPA33–AlexaFluor647 (ref. [50]) and TNFR2–PE–Cy7 monoclonal antibodies as indicated. Detailed information regarding these antibodies can be found in the Reporting Summary. Cells were sorted on a MoFlo Astrios using Summit software version 6.2 (Beckman Coulter) or BD FACS Aria II using FACSDiva software version 8 (BD Biosciences). Propidium iodide (PI) (Sigma) or the Near-IR Dead Cell Stain Kit (Invitrogen) was used to exclude dead cells.

T-cell expansion cultures and restimulation. Sorted human T_{conv} and tT_{reg} cells were plated in 96-well round-bottom plates (Greiner; 1×10^4 cells per well) and cultured in IMDM (Gibco, Life Technologies), supplemented with 8% FCS (Sigma), penicillin/streptomycin (Roche) and 300 IU ml^{-1} IL-2 (DuPont Medical) (T-cell medium) at 37 °C/5% CO_2. Activating monoclonal antibodies against CD3 (clone CLB-T3/4.E, IgE isotype, Sanquin, 0.1 μg ml^{-1}) and CD28 (clone CLB-CD28/1, Sanquin, 0.2 μg ml^{-1}) were added in solution for T-cell expansion (Extended Data Fig. 2a) (see Reporting Summary for additional details). From day 7 to 14, T cells (5×10^5 cells ml^{-1}) were plated in 24-well plates (Greiner). After 1 or 2 weeks of culture, T_{conv} and tT_{reg} cells (1×10^6 cells ml^{-1}) were cultured in 6-well plates (Corning) for 4 d in fresh T-cell medium supplemented with 300 IU ml^{-1} IL-2, but without anti-CD3–CD28 monoclonal antibodies. Dead cells were removed by Ficoll density gradient centrifugation prior to restimulation experiments. T cells were restimulated using activating monoclonal antibodies against CD3 (0.1 μg ml^{-1}), CD28 (0.2 μg ml^{-1}) or TNFR2 (clone MR2-1, Hycult Biotech; 2.5 μg ml^{-1}, additional information available in the Reporting Summary) added in solution. In some cultures, inhibitors of the hexokinase pathway (2-DG, 25 mM), PI3K (LY294002, 10 μM), NF-κB-inducing kinase (NIK; NIK-SMI1, 5 μM)[56] or mTOR (rapamycin, 100 nM) were added 1 h prior to and during restimulation at indicated concentrations.

Flow cytometry. For cell-surface phenotyping, T cells or PBMCs were washed in PBS/1% FCS and stained in the appropriate combinations with the following monoclonal antibodies: CD3–PE (Dako), CD127–BV711, CD4–BB700, CD25–PE (BD Biosciences), CD3–BV510, CD4–BV510, CD8–AlexaFluor700, TNFR2–PE, TNFR2–PE–Cy7, CD28–PE–Cy5, CD19–BV510 (BioLegend), CD3–FITC, CD4–FITC, CD45RA–FITC and CD8–APC (ImmunoTools). Near-IR Dead Cell Stain Kit (Invitrogen) was used to discriminate between live and dead cells. For intracellular staining, cells were fixed and permeabilized using the FOXP3 Staining Buffer Set (Invitrogen), according to the manufacturer's protocol, and were stained using FOXP3–APC, FOXP3–eFluor450 (Invitrogen), CTLA4–PE–Dazzle594, IKZF2–PEDazzle594 and IKZF2–PE–Cy7 (BioLegend) monoclonal antibodies. For staining of GLUT1, phosphorylated mTOR and phosphorylated S6, cells were fixed and permeabilized using the intracellular fixation and permeabilization buffer set (Invitrogen) according to the manufacturer's protocol, followed by staining

using rabbit anti-GLUT1 (Abcam), p-mTOR (Ser2448)–PE–Cy7 or p-S6 (Ser235/Ser236)–PE (Invitrogen) monoclonal antibodies. Goat anti-rabbit Alexa Fluor 488 (Invitrogen) was used as a secondary antibody, and specific staining was confirmed by Fluorescence Minus One controls. Detailed information regarding all antibodies can be found in the Reporting Summary. Flow cytometry was performed using a BD LSR Fortessa or BD LSR II cell analyser (BD Biosciences), samples were acquired using FACSDiva software version 8 and data were analysed using FlowJo software version 10.5.3. For gating strategies, see Supplementary Fig. 1.

Suppression assay. Whole PBMCs were labelled using CellTrace-Violet (CTV; Invitrogen). In short, PBMCs were washed and resuspended in PBS and incubated for 8 min using 5 µM CTV. Following labelling, an equivalent volume of FCS was added, and cells were washed twice in IMDM/8% FCS. Labelled PBMCs were cocultured with expanded tT_{reg} cells that were prestimulated for 24 h or were not, as indicated. Cell cultures were stimulated using anti-CD3 monoclonal antibodies (0.05 µg ml^{-1}). Proliferation of CD4$^+$ and CD8$^+$ T cells was analysed after 4 d of coculture by flow cytometry on a BD LSR Fortessa or BD LSR II cell analyser. For short-term suppression assays, tT_{reg} cells were prestimulated via CD3 and TNFR2 in the presence or absence of 2-DG (25 mM) for 24 h. Equal numbers of live cells were cocultured overnight with CTV-labelled PBMCs. Cocultures were stained using CD3–FITC, CD69–PerCP–Cy5.5 and CD25–PE monoclonal antibodies. Near-IR Dead Cell Stain Kit (Invitrogen) was used to exclude dead cells. Detailed information regarding these antibodies can be found in the Reporting Summary. The percentage suppression was determined using the formula: 100 – ((MFI of CD25 or CD69 in presence of T_{reg} cells)/(MFI of CD25 or CD69 in absence of T_{reg} cells)) × 100. Flow cytometry was performed using a BD LSR Fortessa or BD LSR II cell analyser (BD Biosciences). Data were analysed using FlowJo software version 10.5.3. For gating strategies, see Supplementary Fig. 1.

Transcriptomics. Expanded T cells (1×10^5) were restimulated for 24 h, washed in ice-cold PBS and resuspended in RLT buffer (Qiagen). Total RNA isolation was performed according to the manufacturer's protocol using the RNeasy MinElute Cleanup Kit (Qiagen), including an on-column DNAse digestion (Qiagen). Quality and quantity of the total RNA were assessed on a 2100 Bioanalyzer using a Nano chip (Agilent). From RNA samples with a measured RNA Integrity Number (RIN) between 8.0 and 10.0, strand-specific libraries were generated using the TruSeq Stranded mRNA sample preparation kit (Illumina), according to manufacturer's instructions (Illumina, part no. 15031047 Rev. E). Polyadenylated RNA from intact total RNA was purified using oligo-dT beads. Following purification, the RNA was fragmented, randomly primed and reverse-transcribed using SuperScript II Reverse Transcriptase (Invitrogen). Second-strand synthesis was performed using polymerase I and RNase H with replacement of dTTP for dUTP. The generated complementary DNA fragments were 3′-end adenylated and ligated to Illumina paired-end sequencing adapters and subsequently amplified by 12 cycles of PCR. The libraries were analysed on a 2100 Bioanalyzer using a 7500 chip (Agilent), diluted and pooled in equimolar ratios into a multiplex sequencing pool. The pooled libraries were eventually sequenced with 65-base single reads on a HiSeq2500 using V4 chemistry (Illumina).

RNA-sequencing analysis. The 65-bp single-end reads were mapped to the human reference genome (hg38) using TopHat (version 2.1.0), which allows exon–exon splice junctions to be spanned. TopHat was supplied with a known set of gene models based on Ensembl gene transfer format (GTF) version 77. The samples were generated using a stranded protocol, which means that TopHat was guided to use the first strand as the library type. Furthermore, TopHat was run with Bowtie 1 and uses the prefilter multihits and no coverage as additional arguments. In order to count the number of reads per gene, a custom script (Itreecount) was used. This script is based on the same ideas as HTSeq-count and has comparable output. Itreecount generates a list of the total number of uniquely mapped sequencing reads for each gene that is present in the GTF file.

Differential-expression analysis and hierarchical clustering were performed in Qlucore Omics Explorer (version 3.4), using the trimmed mean of log expression ratios method (TMM). GRCh38.77.gtf was used as reference genome for alignment. Genes were excluded from downstream expression analysis if they failed to have ten reads in at least six samples. Differential expression with a two-group comparison (Student's *t* test with the Benjamini–Hochberg method for multiple testing correction) was considered significant at FDR < 0.05. For a multigroup comparison (ANOVA with the Benjamini–Hochberg method), the threshold was set at FDR < 0.005. PCA was used to visualize the data set in three-dimensional space, after filtering out variables with low overall variance due to the impact of noise and centering and scaling the remaining variables to zero mean and unit variance.

TPM were calculated following read count and length normalization for individual genes for each RNA-sequencing sample using R (version 3.5.1). Only the genes with a CPM value >2 in all samples were subjected to differential-expression analysis. MA plots were generated following edgeR (version 3.8.6) normalization and exact test[57,58], in which genes with FDR < 0.01 were considered differentially expressed. The FRY test[59] (limma[60], version 3.22.7), which is a fast approximation to ROAST, was used to test for enrichment of a-priori-defined gene sets among genes that are high- or low-ranked on the basis of differential expression between two biological states. This test was performed on edgeR-normalized data to compare the gene-expression profiles of CD3- or CD3–TNFR2-activated tT_{reg} cells with those of unstimulated or CD3–CD28-activated T_{conv} cells. Data were depicted as a barcode plot including an enrichment score. In addition, GSEA software (version 4.0.0, http://broadinstitute.org/gsea) was employed to test the hallmark gene-set collection (Molecular Signatures Database; MSigDB[61]) for enrichment in the gene-expression profiles of CD3- or CD3–TNFR2-activated tT_{reg} cells, using CPM, to identify involved biological processes.

Along with GSEA, IPA (version 52912811, Qiagen) was used to identify biological processes that were affected by differentially expressed genes between tT_{reg} cells that were activated via CD3 or CD3 and TNFR2 for 24 h as determined by Qlucore Omics Explorer (FDR < 0.05). Pathways were tested for enrichment using the right-tailed Fisher's exact test with the Benjamini–Hochberg method (FDR < 0.05). Detailed information regarding software can be found in the Reporting Summary.

LC–MS and metabolomics. Expanded T cells (5×10^5) were restimulated, collected after 24 h and centrifuged for 5 min at 1,000*g*. Medium samples were collected and cell pellets were washed with ice-cold PBS. For metabolic-flux analysis, medium was formulated to match the composition of IMDM. Medium consisted of DMEM (lacking glucose and pyruvate), supplemented with additional non-essential amino acids, 1 mM pyruvate, 25 mM U-$^{13}C_6$-labelled D-glucose (Cambridge Isotopes), 8% FCS (Sigma) and penicillin/streptomycin. T cells (5×10^5) were cultured at a density of 1×10^6 cells ml^{-1} for 24 h prior to collection. Metabolites were extracted by adding 50 µl ice-cold MS lysis buffer (2:2:1 methanol/acetonitrile/ultrapure LC–MS-grade water) to the cell pellet. Extracellular metabolites were extracted by adding 25 µl medium to 100 µl methanol/acetonitrile (1:1). Samples were shaken for 10 min at 4 °C and centrifuged at 14,000*g* for 15 min at 4 °C, and supernatants were collected for LC–MS analysis. LC–MS analysis was performed on an Exactive mass spectrometer (Thermo Scientific) coupled to a Dionex Ultimate 3000 autosampler and pump (Thermo Scientific). The MS operated in polarity-switching mode with spray voltages of 4.5 kV and −3.5 kV. Metabolites were separated using a Sequant ZIC-pHILIC column (2.1 × 150 mm, 5 µm, guard column 2.1 × 20 mm, 5 µm; Merck) using a linear gradient of acetonitrile and eluent A (20 mM $(NH_4)_2CO_3$, 0.1% NH_4OH in ultrapure LC–MS-grade water; Biosolve). Flow rate was set at 150 µl min^{-1}. Metabolites were identified on the basis of exact mass within 5 ppm and were further validated by concordance with retention times of standards. Metabolites were quantified using LCquan software (Thermo Scientific, version 2.9). Cells were resuspended at equal cell densities, and no cell growth occurred in T cells up to 24 h after restimulation. Therefore, samples were assumed to contain equal cell numbers. To correct for technical variations during mass-spectrometry analysis, peak areas of intracellular metabolites were additionally normalized on the basis of total peak intensity of all identified metabolites (untargeted metabolomics) or essential amino acids (metabolic-flux analysis). Isotopomer distributions were corrected for natural abundance.

For targeted metabolomics of freshly isolated T cells (5×10^5) (Fig. 8h), metabolites were extracted from cells as indicated above, with 2:2:1 methanol/acetonitrile/water. The supernatant was dried under nitrogen, reconstituted in 60 µl water and ultrasonicated for 5 min. Per sample, 10 µl was used for analysis. According to Ross et. al.[62], ultra-high-performance liquid chromatography was done using a Phenomenex Aqua C18 column (Phenomenex) on a Nexera X2 system (Shimadzu). The column was eluted with a gradient of water with 0.1% formic acid (LC–MS 98%, Honeywell, Fluka; eluent A) and acetonitrile with 0.1% formic acid (eluent B) with a column flow of 400 µl min^{-1} as follows: 0 min 0% B, 3.5 min 0% B, 4 min 90% B, 5 min 90% B. Ensuing MS was performed on a Sciex TripleTOF 6600 (AB Sciex) operated in negative ESI mode, with ion source gas 1, 45 psi; ion source gas 2, 50 psi; curtain gas, 35 psi; temperature, 500 °C; acquisition range, *m/z* 50–1,000; ion-spray voltage, −4,500 V; declustering potential, −80.0 V. An information-dependent acquisition (IDA) scan was done to confirm the identity of the glycolysis intermediates, with the following conditions: collision energy, −10; acquisition time, 250 ms. For tandem MS analysis: collision energy, −30; collision energy spread, 15; ion-release delay, 30; ion-release width, 14; acquisition time, 40 ms. The IDA switching criteria were set as follows: for ions smaller than *m/z* 600, which exceed 200 counts per second, never exclude former target ions, exclude isotopes within 2 Da, maximum number of candidate ions: 20. Standards for quality control of F-1,6-BP and lactate were purchased from Merck Chemicals. Tandem mass spectra were curated with PeakView (version 2.2.0, AB Sciex) and manually compared with spectra in the Metlin metabolite database[63,64]. MultiQuant (version 3.0.3. AB Sciex) was used for peak integration. Peak areas were normalized to the cell count obtained after cell sorting.

Glucose-uptake assay. T cells (5×10^4) were stimulated using CD3-, CD28- or TNFR2-activating monoclonal antibodies for 24 h, as indicated. Cells were washed in DMEM without glucose and phenol red (Gibco), followed by incubation with 6-NBDG (100 µM, Invitrogen) in DMEM without glucose and phenol red for 45 min at 37 °C and 5% CO_2. For 6-NBDG-uptake assays using freshly sorted cells, T cells were incubated directly after flow-cytometric sorting for 1 h in DMEM without glucose and phenol red, supplemented with 1% FCS. For glucose uptake,

6-NBDG was added directly to the culture for an additional 45 min. Cells were washed once in PBS with 2% FCS, followed by acquisition of the samples using a BD LSR Fortessa or BD LSR II cell analyser. DAPI (Stem Cell Technologies) or PI was used to exclude dead cells. For gating strategies, see Supplementary Fig. 1.

Confocal laser scanning microscopy. For imaging, T cells (5×10^4) were stimulated using CD3-, CD28- or TNFR2-activating monoclonal antibodies for 24 h, as indicated. Cells were stained on the plasma membrane using CD45–PE–CF594 (BD Biosciences). After cell fixation and permeabilization, GLUT1 was stained using rabbit anti-GLUT1 (Abcam) and goat anti-rabbit Alexa Fluor 488 (Invitrogen) as a secondary antibody (see Reporting Summary for additional information). Counterstaining of the nucleus was performed using DAPI (Sigma). Cells were suspended in PBS and added to 35/10-mm glass-bottom dishes (Greiner Bio-One). Images were acquired on the Andor Dragonfly 505 spinning disk confocal microscope adapted with a Leica DMi8 microscope (Oxford Instruments) at ×63 magnification. Image processing was performed using Fiji/ImageJ software (version 1.52j), and colocalization, reported as Pearson's *r*, was calculated on a single-cell basis using the JACoP plug-in (see Reporting Summary).

Seahorse metabolic assays. Real-time metabolic analyses were performed using a Seahorse XFe24 analyser (Agilent Technologies)[65]. For this purpose, 5×10^5 T cells were plated on poly-D-lysine-coated (Sigma) plates. After baseline measurement according to the manufacturer's protocol, cells were stimulated via injection port A containing CD3-, CD28- and TNFR2-activating monoclonal antibodies, and ECAR measurements were done for 15 cycles of 3 min mixing, 2 min waiting and 3 min measuring. Data were analysed using Wave software version 2.6.0.31 (Agilent Technologies). The area under the curve (AUC) of the ECAR in time following stimulation was determined by normalizing to the baseline ECAR measurement.

Methylation analysis of the TSDR. Expanded T cells (2.5×10^4 cells) were restimulated overnight as indicated. Bisulfite conversion of DNA was performed using the EZ DNA Methylation-Direct kit (Zymo Research) according to the manufacturer's protocol. Cell pellets were taken up in PBS for proteinase K digestion. Methylation-specific (MS) quantitative PCR (qPCR) was performed using iQ SYBR Green Supermix (Bio-Rad)[66]. MS–qPCR was performed in 8-µl reactions, containing 2 µl of bisulfite-treated DNA solution, 0.5 µM of methylation- or demethylation-specific primers for the *FOXP3* TSDR and 4 µl SYBR Green reagent (Bio-Rad). Methylation-specific primers were 5′-CGATAGGGTAGTTAGTTTTCGGAAC-3′ and 5′-CATTAACGTCATAACGACCGAA-3′; demethylation-specific primers were 5′-TAGGGTAGTTAGTTTTTGGAATGA-3′ and 5′-CCATTAACATCATAACAACCAAA-3′. MS–qPCR was conducted at 98 °C for 10 min, then 40 cycles of 98 °C for 15 s and 60 °C for 1 min, which was followed by melt-curve analysis on a LightCycler 480-II (Roche). Methylation of the TSDR (%) was calculated using the following formula: $100/(1 + 2^{Ct(CG) - Ct(TG)})$, where Ct(CG) is defined as Ct values obtained using methylation-specific primers and Ct(TG) is defined as Ct values obtained using demethylation-specific primers.

Statistical analysis. Data, excluding those describing transcriptomics or metabolomics data, were analysed using GraphPad Prism, version 8.1.1. Statistical analyses were performed as indicated in the figure legends. Data were log-transformed in case data were not normally distributed. Data are represented as mean ± s.e.m. A two-sided $P < 0.05$ was considered statistically significant.

Reporting Summary. Further information on research design is available in the Nature Research Reporting Summary linked to this article.

Data availability

All RNA-seq data are available in the GEO database under accession code GSE138603 and GSE138604. GSEAs were performed with GSEA software using the hallmark gene sets listed in the Molecular Signatures Database (MSigDB) available through https://www.gsea-msigdb.org/gsea/index.jsp. The proteomics data set used in this study is published by Cuadrado et al.[14]. All other data that support the findings of this study are available from the corresponding author on reasonable request.

Code availability

For RNA-sequencing, the script Itreecount was used to count the number of reads per gene. Itreecount is publicly available through https://github.com/NKI-GCF/itreecount.

Received: 25 September 2019; Accepted: 27 July 2020;
Published online: 21 September 2020

References

1. Wing, J. B., Tanaka, A. & Sakaguchi, S. Human FOXP3$^+$ regulatory T cell heterogeneity and function in autoimmunity and cancer. *Immunity* **50**, 302–316 (2019).
2. Shevach, E. M. & Thornton, A. M. tT$_{reg}$s, pT$_{reg}$s, and iT$_{reg}$s: similarities and differences. *Immunol. Rev.* **259**, 88–102 (2014).
3. Fontenot, J. D., Gavin, M. A. & Rudensky, A. Y. Foxp3 programs the development and function of CD4$^+$CD25$^+$ regulatory T cells. *Nat. Immunol.* **4**, 330–336 (2003).
4. Hori, S., Nomura, T. & Sakaguchi, S. Control of regulatory T cell development by the transcription factor Foxp3. *Science* **299**, 1057–1061 (2003).
5. Floess, S. et al. Epigenetic control of the foxp3 locus in regulatory T cells. *PLoS Biol.* **5**, e38 (2007).
6. Blazar, B. R., MacDonald, K. P. A. & Hill, G. R. Immune regulatory cell infusion for graft-versus-host disease prevention and therapy. *Blood* **131**, 2651–2660 (2018).
7. Riley, J. L., June, C. H. & Blazar, B. R. Human T regulatory cell therapy: take a billion or so and call me in the morning. *Immunity* **30**, 656–665 (2009).
8. Koenen, H. J. et al. Human CD25^{high}Foxp3^{pos} regulatory T cells differentiate into IL-17-producing cells. *Blood* **112**, 2340–2352 (2008).
9. Medler, J. & Wajant, H. Tumor necrosis factor receptor-2 (TNFR2): an overview of an emerging drug target. *Expert Opin. Ther. Targets* **23**, 295–307 (2019).
10. Salomon, B. L. et al. Tumor necrosis factor alpha and regulatory T cells in oncoimmunology. *Front. Immunol.* **9**, 444 (2018).
11. Huynh, A. et al. Control of PI(3) kinase in T$_{reg}$ cells maintains homeostasis and lineage stability. *Nat. Immunol.* **16**, 188–196 (2015).
12. Zeiser, R. et al. Differential impact of mammalian target of rapamycin inhibition on CD4$^+$CD25$^+$Foxp3$^+$ regulatory T cells compared with conventional CD4$^+$ T cells. *Blood* **111**, 453–462 (2008).
13. Sauer, S. et al. T cell receptor signaling controls Foxp3 expression via PI3K, Akt, and mTOR. *Proc. Natl Acad. Sci. USA* **105**, 7797–7802 (2008).
14. Cuadrado, E. et al. Proteomic analyses of human regulatory T cells reveal adaptations in signaling pathways that protect cellular identity. *Immunity* **48**, 1046–1059 (2018).
15. Menk, A. V. et al. Early TCR signaling induces rapid aerobic glycolysis enabling distinct acute T cell effector functions. *Cell Rep.* **22**, 1509–1521 (2018).
16. Frauwirth, K. A. et al. The CD28 signaling pathway regulates glucose metabolism. *Immunity* **16**, 769–777 (2002).
17. Basu, S., Hubbard, B. & Shevach, E. M. Foxp3-mediated inhibition of Akt inhibits Glut1 (glucose transporter 1) expression in human T regulatory cells. *J. Leukoc. Biol.* **97**, 279–283 (2015).
18. Michalek, R. D. et al. Cutting edge: distinct glycolytic and lipid oxidative metabolic programs are essential for effector and regulatory CD4$^+$ T cell subsets. *J. Immunol.* **186**, 3299–3303 (2011).
19. Shi, L. Z. et al. HIF1alpha-dependent glycolytic pathway orchestrates a metabolic checkpoint for the differentiation of T$_H$17 and T$_{reg}$ cells. *J. Exp. Med.* **208**, 1367–1376 (2011).
20. He, N. et al. Metabolic control of regulatory T cell (T$_{reg}$) survival and function by Lkb1. *Proc. Natl Acad. Sci. USA* **114**, 12542–12547 (2017).
21. Beier, U. H. et al. Essential role of mitochondrial energy metabolism in Foxp3$^+$ T-regulatory cell function and allograft survival. *FASEB J.* **29**, 2315–2326 (2015).
22. Angelin, A. et al. Foxp3 reprograms T cell metabolism to function in low-glucose, high-lactate environments. *Cell Metab.* **25**, 1282–1293 e1287 (2017).
23. Gerriets, V. A. et al. Foxp3 and Toll-like receptor signaling balance T$_{reg}$ cell anabolic metabolism for suppression. *Nat. Immunol.* **17**, 1459–1466 (2016).
24. Howie, D. et al. Foxp3 drives oxidative phosphorylation and protection from lipotoxicity. *JCI Insight* **2**, e89160 (2017).
25. Delgoffe, G. M. et al. The kinase mTOR regulates the differentiation of helper T cells through the selective activation of signaling by mTORC1 and mTORC2. *Nat. Immunol.* **12**, 295–303 (2011).
26. Wei, J. et al. Autophagy enforces functional integrity of regulatory T cells by coupling environmental cues and metabolic homeostasis. *Nat. Immunol.* **17**, 277–285 (2016).
27. Chapman, N. M. et al. mTOR coordinates transcriptional programs and mitochondrial metabolism of activated T$_{reg}$ subsets to protect tissue homeostasis. *Nat. Commun.* **9**, 2095 (2018).
28. Procaccini, C. et al. The proteomic landscape of human ex vivo regulatory and conventional T cells reveals specific metabolic requirements. *Immunity* **44**, 712 (2016).
29. De Rosa, V. et al. Glycolysis controls the induction of human regulatory T cells by modulating the expression of FOXP3 exon 2 splicing variants. *Nat. Immunol.* **16**, 1174–1184 (2015).
30. Yang, S., Wang, J., Brand, D. D. & Zheng, S. G. Role of TNF–TNF receptor 2 Signal in regulatory T cells and Its therapeutic implications. *Front. Immunol.* **9**, 784 (2018).
31. Atretkhany, K. N. et al. Intrinsic TNFR2 signaling in T regulatory cells provides protection in CNS autoimmunity. *Proc. Natl Acad. Sci. USA* **115**, 13051–13056 (2018).
32. Marin Morales, J. M. et al. Automated clinical grade expansion of regulatory T cells in a fully closed system. *Front. Immunol.* **10**, 38 (2019).

33. Opstelten, R. et al. GPA33: A marker to identify stable human regulatory T cells. *J. Immunol.* **204**, 3139–3148 (2020).
34. Zheng, Y. et al. Genome-wide analysis of Foxp3 target genes in developing and mature regulatory T cells. *Nature* **445**, 936–940 (2007).
35. Golovina, T. N. et al. CD28 costimulation is essential for human T regulatory expansion and function. *J. Immunol.* **181**, 2855–2868 (2008).
36. Tanner, L. B. et al. Four key steps control glycolytic flux in mammalian cells. *Cell Syst.* **7**, 49–62 e48 (2018).
37. Gerriets, V. A. et al. Metabolic programming and PDHK1 control $CD4^+$ T cell subsets and inflammation. *J. Clin. Invest.* **125**, 194–207 (2015).
38. Shi, J. H. & Sun, S. C. Tumor necrosis factor receptor-associated factor regulation of nuclear factor κB and mitogen-activated protein kinase pathways. *Front. Immunol.* **9**, 1849 (2018).
39. He, X. et al. A TNFR2-agonist facilitates high purity expansion of human low purity treg cells. *PLoS ONE* **11**, e0156311 (2016).
40. Macintyre, A. N. et al. The glucose transporter Glut1 is selectively essential for CD4 T cell activation and effector function. *Cell Metab.* **20**, 61–72 (2014).
41. Hui, S. et al. Glucose feeds the TCA cycle via circulating lactate. *Nature* **551**, 115–118 (2017).
42. Vander Heiden, M. G., Cantley, L. C. & Thompson, C. B. Understanding the Warburg effect: the metabolic requirements of cell proliferation. *Science* **324**, 1029–1033 (2009).
43. Haas, R. et al. Intermediates of metabolism: from bystanders to signalling molecules. *Trends Biochem. Sci.* **41**, 460–471 (2016).
44. Acuto, O. & Michel, F. CD28-mediated co-stimulation: a quantitative support for TCR signalling. *Nat. Rev. Immunol.* **3**, 939–951 (2003).
45. Walker, L. S. & Sansom, D. M. Confusing signals: recent progress in CTLA-4 biology. *Trends Immunol.* **36**, 63–70 (2015).
46. Grell, M. et al. The transmembrane form of tumor necrosis factor is the prime activating ligand of the 80 kDa tumor necrosis factor receptor. *Cell* **83**, 793–802 (1995).
47. Urbano, P. C. M., Koenen, H., Joosten, I. & He, X. An autocrine TNFα-tumor necrosis factor receptor 2 loop promotes epigenetic effects inducing human treg stability in vitro. *Front. Immunol.* **9**, 573 (2018).
48. Kleijwegt, F. S. et al. Critical role for tnf in the induction of human antigen-specific regulatory T cells by tolerogenic dendritic cells. *J. Immunol.* **185**, 1412 (2010).
49. Chopra, M. et al. Exogenous TNFR2 activation protects from acute GvHD via host T reg cell expansion. *J. Exp. Med.* **213**, 1881–1900 (2016).
50. Herbertson, R. A. et al. Targeted chemoradiation in metastatic colorectal cancer: a phase I trial of 131I-huA33 with concurrent capecitabine. *J. Nucl. Med.* **55**, 534–539 (2014).
51. Zhang, D. et al. Metabolic regulation of gene expression by histone lactylation. *Nature* **574**, 575–580 (2019).
52. Williams, N. C. & O'Neill, L. A. J. A role for the Krebs cycle intermediate citrate in metabolic reprogramming in innate immunity and inflammation. *Front. Immunol.* **9**, 141 (2018).
53. Thurnher, M. & Gruenbacher, G. T lymphocyte regulation by mevalonate metabolism. *Sci. Signal* **8**, re4 (2015).
54. Timilshina, M. et al. Activation of mevalonate pathway via LKB1 is essential for stability of treg cells. *Cell Rep.* **27**, 2948–2961 e2947 (2019).
55. Zeng, H. et al. mTORC1 couples immune signals and metabolic programming to establish T_{reg}-cell function. *Nature* **499**, 485–490 (2013).
56. Brightbill, H. D. et al. NF-κB inducing kinase is a therapeutic target for systemic lupus erythematosus. *Nat. Commun.* **9**, 179 (2018).
57. McCarthy, D. J., Chen, Y. & Smyth, G. K. Differential expression analysis of multifactor RNA-seq experiments with respect to biological variation. *Nucleic Acids Res.* **40**, 4288–4297 (2012).
58. Robinson, M. D., McCarthy, D. J. & Smyth, G. K. edgeR: a Bioconductor package for differential expression analysis of digital gene expression data. *Bioinformatics* **26**, 139–140 (2010).
59. Chen, Y., Lun, A. & Smyth, G. From reads to genes to pathways: differential expression analysis of RNA-seq experiments using Rsubread and the edgeR quasi-likelihood pipeline. *F1000Res* **5**, 1438 (2016).
60. Ritchie, M. E. et al. limma powers differential expression analyses for RNA-sequencing and microarray studies. *Nucleic Acids Res.* **43**, e47 (2015).
61. Liberzon, A. et al. The molecular signatures database hallmark gene set collection. *Cell Syst.* **1**, 417–425 (2015).
62. Ross, K. L. & Dalluge, J. J. Liquid chromatography/tandem mass spectrometry of glycolytic intermediates: deconvolution of coeluting structural isomers based on unique product ion ratios. *Anal. Chem.* **81**, 4021–4026 (2009).
63. Smith, C. A. et al. METLIN: a metabolite mass spectral database. *Ther. Drug Monit.* **27**, 747–751 (2005).
64. Guijas, C. et al. METLIN: a technology platform for identifying knowns and unknowns. *Anal. Chem.* **90**, 3156–3164 (2018).
65. van der Windt, G. J., Chang, C. H. & Pearce, E. L. Measuring bioenergetics in T cells using a seahorse extracellular flux analyzer. *Curr. Protoc. Immunol.* **113**, 3.16B.11–13.16B.14 (2016).
66. Zhuo, C. et al. Higher FOXP3–TSDR demethylation rates in adjacent normal tissues in patients with colon cancer were associated with worse survival. *Mol. Cancer* **13**, 153 (2014).

Acknowledgements

We thank the employees of the Flow Cytometry Facility and Genomics Facility of the Netherlands Cancer Institute and the Flow Cytometry Core Facility at Leiden University Medical Center for their technical assistance, M. Giera and S. Kostidis of the Center for Proteomics and Metabolomics Facility at Leiden University Medical Center for valuable discussions regarding the metabolomics experiments on freshly sorted cells and E. Schrama for assistance in flow-cytometric assays. M. A. Aslam was supported by the Institute of Molecular Biology and Biotechnology, Bahauddin Zakariya University, Multan, Pakistan. This work was supported by Oncode, ZonMW-TOP grant 40-00812-98-13071 and grants ICI-00014 and ICI-00025 from the Institute for Chemical Immunology, funded by ZonMW Gravitation.

Author contributions

S.d.K., M.M., J.B. and C.R.B. designed the study; S.d.K., M.M. and A.T.H. designed and performed the experiments and analysed the data; I.B. performed confocal microscopy experiments, analysed the data and contributed to the manuscript; R.J.E.D. performed targeted metabolomics analysis on freshly sorted cells and contributed to the manuscript; D.B. performed the short-term metabolic assays; M.A.A. provided assistance in analyses of the transcriptome data; S.d.K., M.M., J.B. and C.R.B. wrote the manuscript; D.A. provided conceptual advice in the study design and contributed to writing the manuscript.

Competing interests

All authors declare to have no financial or non-financial competing interests.

Additional information

Extended data is available for this paper at https://doi.org/10.1038/s42255-020-00271-w.

Supplementary information is available for this paper at https://doi.org/10.1038/s42255-020-00271-w.

Correspondence and requests for materials should be addressed to C.R.B. or J.B.

Peer review information Primary Handling Editors: George Caputa; Elena Bellafante.

Reprints and permissions information is available at www.nature.com/reprints.

Publisher's note Springer Nature remains neutral with regard to jurisdictional claims in published maps and institutional affiliations.

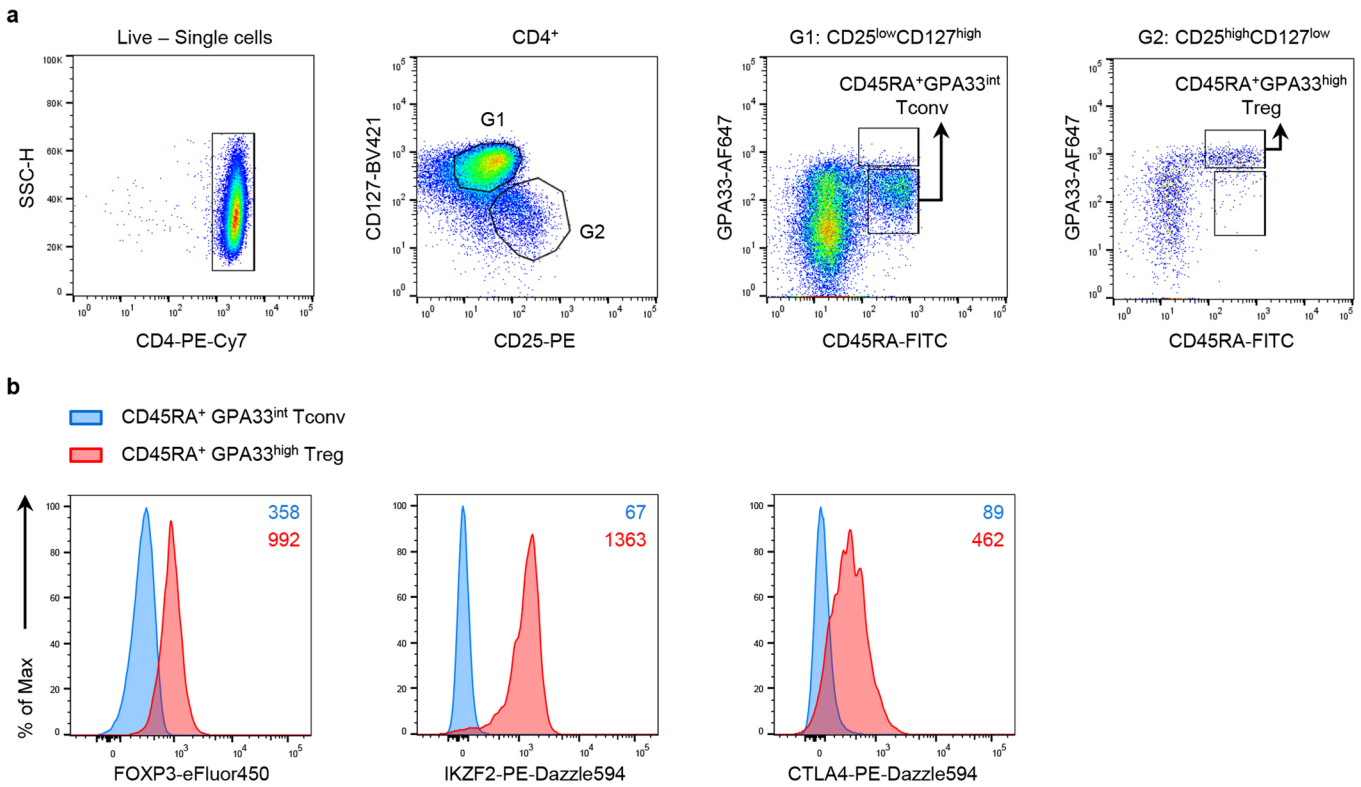

Extended Data Fig. 1 | Cell sorting strategy and characterization of naïve CD4⁺ Tconv and tTreg cells from human peripheral blood. a, Total human CD4⁺ T cells were isolated from human PBMC using MACS and subjected to fluorescence-activated cell sorting. Within the live (PI^-) and single cell gates (FSC-A/FSC-H), CD4⁺ T cells were selected for further discrimination between Tconv and tTreg cells using CD127 and CD25 expression levels (G1 and G2). Subsequently, naïve Tconv and tTreg cells were gated based on CD45RA expression and the novel marker GPA33 to obtain tTreg cells with high purity, resulting in $CD25^{low}CD127^{high}CD45RA^{+}GPA33^{int}$ Tconv cells and $CD25^{high}CD127^{low}CD45RA^{+}GPA33^{high}$ tTreg cells. **b**, Flow cytometric analysis of FOXP3, IKZF2 and total CTLA4 protein expression in the naïve Tconv and tTreg cells (representative of n=6). Mean fluorescence intensity (MFI) is shown in the plots. Sample size (n) represents cells from individual donors, analyzed in independent experiments.

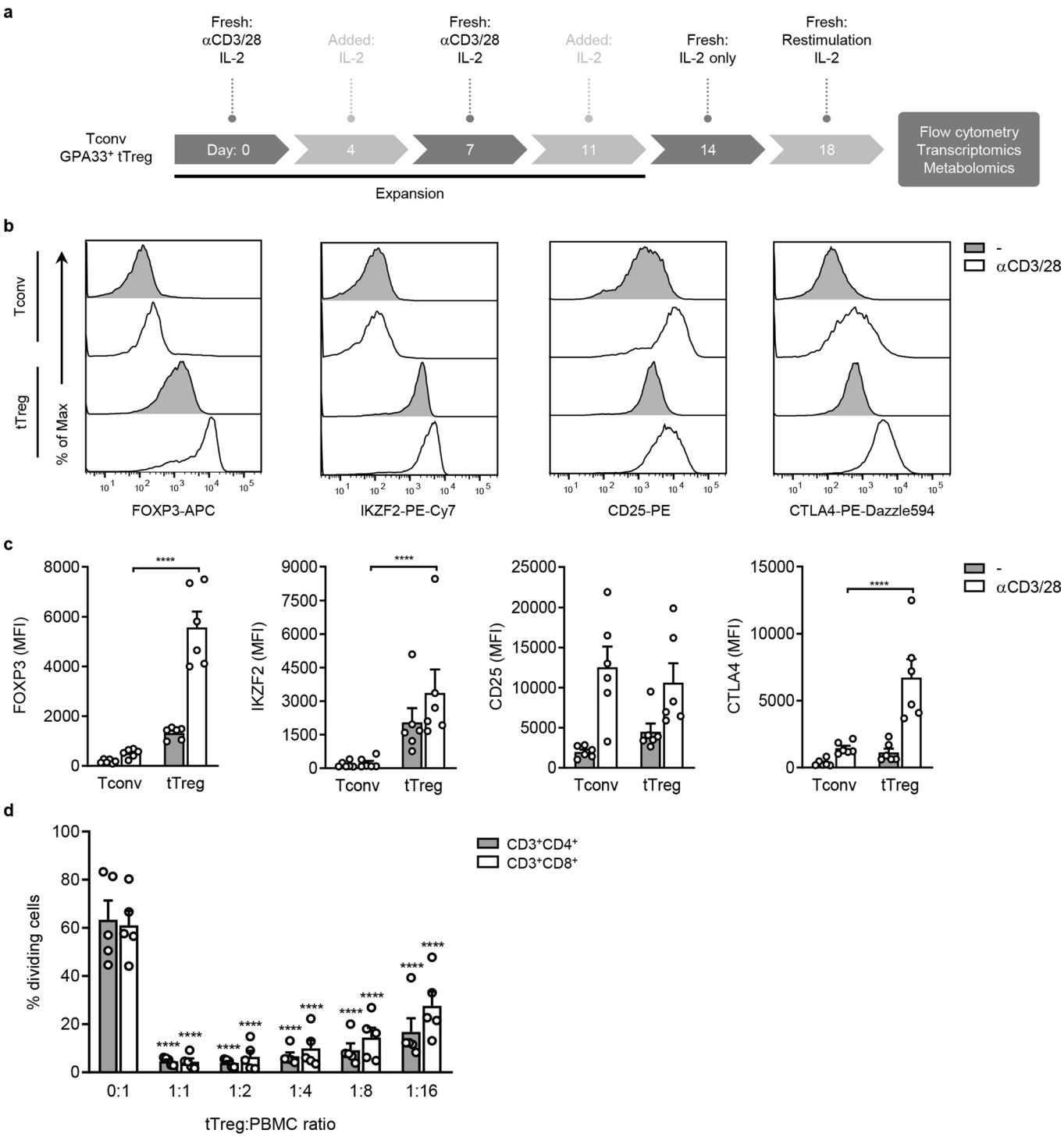

Extended Data Fig. 2 | Phenotypical and functional characterization of *in vitro* expanded Tconv and tTreg cells. a, Schematic overview of Tconv and tTreg cell expansion cultures. The nature of "restimulation" on day 18 is indicated in the legends of the specific experiments. **b**, Flow cytometric analysis of FOXP3, IKZF2, cell surface CD25 and total CTLA4 protein levels in expanded Tconv and tTreg cells at 24 h after restimulation with anti-CD3/CD28 mAbs or control (-) (representative of n=6). **c**, Quantification of flow cytometric results obtained as indicated in **b**, showing the MFI for each protein (n=6), ****p=5.02x10^{-5}, 3.34x10^{-6} and 5.58x10^{-5} for FOXP3, IKZF2 and CTLA4, respectively. **d**, Assessment of the suppressive capacity of tTreg cells on day 18 of the expansion cultures. Cells in the suppression assay were stimulated with agonistic mAb to CD3 and the assay was read out after 4 days. The percentage of dividing CD4$^+$ and CD8$^+$ Tconv cells is displayed (n=5), ****p=5.1x10^{-13}, 4.99x10^{-13}, 5.57x10^{-13}, 8.67x10^{-13} and 3.32x10^{-11} for 1:1, 1:2, 1:4, 1:8 and 1:16 ratio versus 0:1 ratio, respectively, within CD3$^+$CD4$^+$ responder cells and ****p=5.81x10^{-13}, 7.83x10^{-13}, 2.67x10^{-12}, 3.4x10^{-11} and 1.78x10^{-7} for 1:1, 1:2, 1:4, 1:8 and 1:16 ratio versus 0:1 ratio, respectively, within CD3$^+$CD8$^+$ responder cells. (**c**, **d**) Two-way ANOVA with Tukey's *post hoc* test was used for statistical analysis. Data are presented as mean ± SEM. Sample size (n) represents cells from individual donors, analyzed in independent experiments (**a**–**d**).

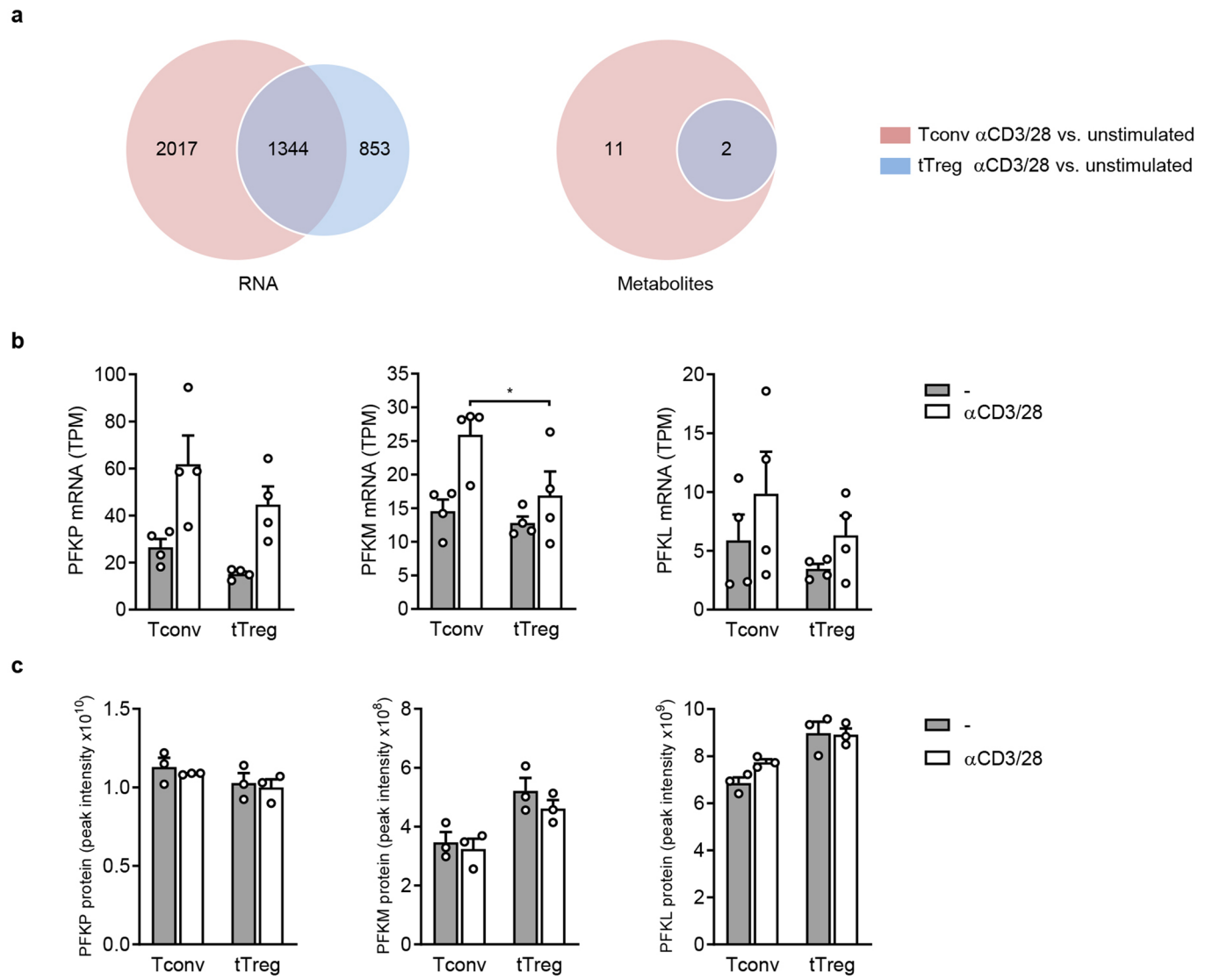

Extended Data Fig. 3 | PFK mRNA and protein expression by Tconv and tTreg cells upon CD3/CD28-mediated activation. a, Venn diagrams depicting the number of overlapping and unique genes (left) or metabolites (right) that showed significant changes in abundance upon CD3/CD28-mediated activation for 24 h in Tconv and tTreg cells, as determined by transcriptomics and metabolomics (n=4). Statistical evaluation was performed using an unpaired two-sided Student's t-test with the Benjamini-Hochberg method with FDR<0.05 (transcriptomics) or by unpaired two-sided Student's t-test with p<0.05 (metabolomics). **b**, mRNA (top) and protein levels (bottom) of PFK isoforms in Tconv and tTreg cells at 24 h after stimulation as indicated. mRNA levels are expressed in TPM, as detected in our transcriptome data set (n=4), *p=0.0408. (**c**) Protein levels are expressed in LFQ intensity, as detected in an earlier proteomics data set[14] (n=3). (**b**, **c**) Two-way ANOVA with Bonferroni's *post hoc* test was used for statistical analysis. Data are presented as mean ± SEM. Sample size (n) represents independent expansion cultures of distinct donors (**a**–**c**).

Glycolysis/TCA cycle intermediates in unstimulated vs αCD3/CD28 in Tconv cells			
Metabolite	**Pathway/Process**	***p*-value***	**Log_2 fold change**
HexoseP	Glycolysis	0.0260	1.739
Glyceraldehyde3P	Glycolysis	0.0140	2.475
Dihydroxyacetone3P	Glycolysis	0.0179	3.352
Lactate	Glycolysis	0.0193	1.039
α-Ketoglutarate	TCA cycle	0.0440	1.426

Glycolysis/TCA cycle intermediates in unstimulated vs αCD3/CD28 in tTreg cells			
Metabolite	**Pathway/Process**	***p*-value***	**Log_2 fold change**
Dihydroxyacetone3P	Glycolysis	0.0288	2.169

Extended Data Fig. 4 | Significant changes in glycolysis/TCA cycle intermediates in Tconv and tTreg cells activated via CD3/CD28. Unpaired two-sided Student's *t*-test was used for statistical analysis (*). Data is derived from 4 independent expansion cultures of distinct donors.

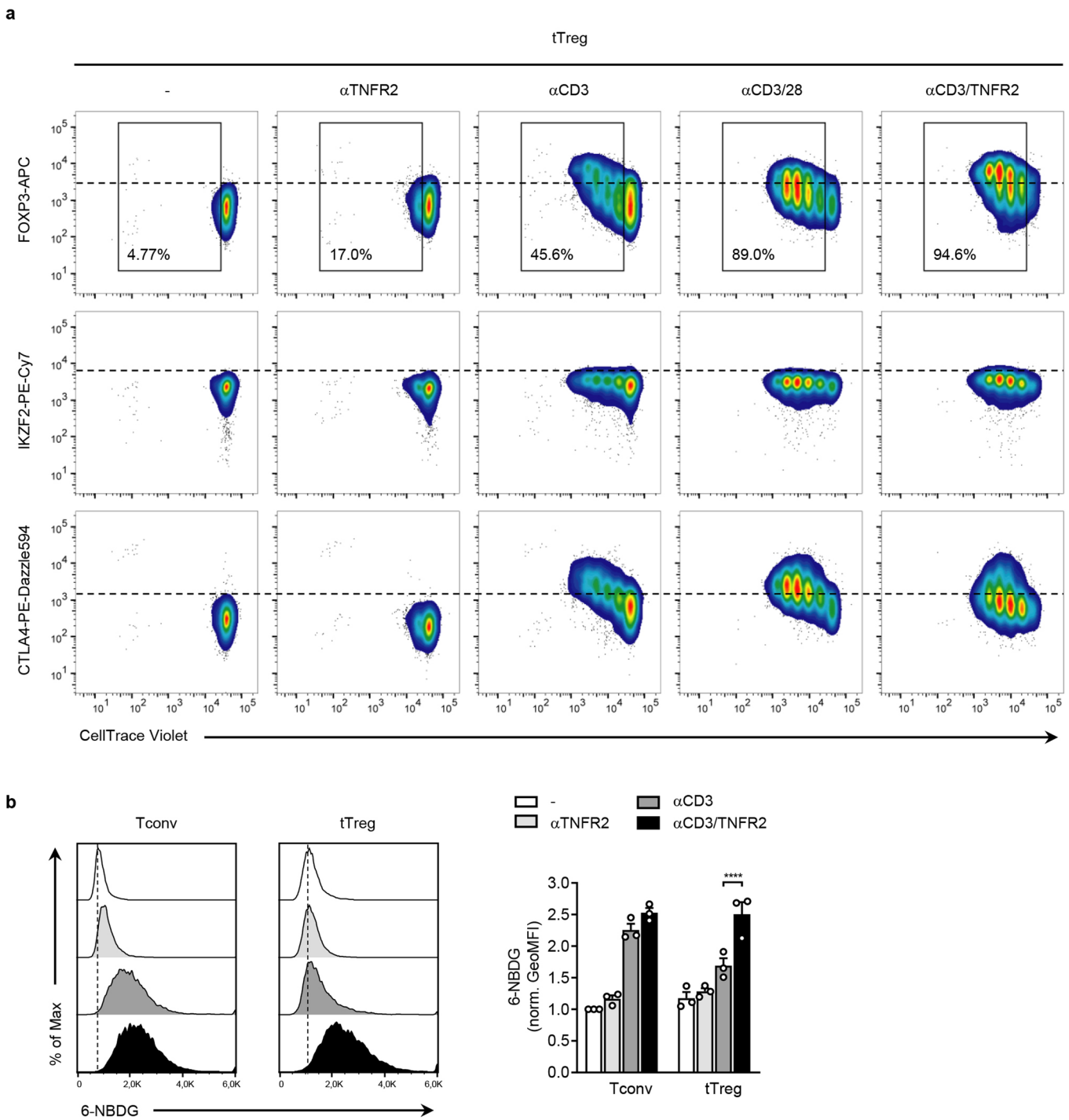

Extended Data Fig. 5 | TNFR2 acts as a costimulatory receptor on tTreg cells. a, Flow cytometric assessment of tTreg cell division by CTV dilution upon restimulation for 96 h as indicated. The percentage of dividing cells is depicted. FOXP3, IKZF2 and total CTLA4 protein expression is shown for each cell division (representative of n=3). **b**, Left panel: Flow cytometric assessment of 6-NBDG uptake activity in Tconv and tTreg cells that were restimulated for 24 h as indicated. Dashed lines indicate the modal 6-NBDG uptake for unstimulated cells. Right panel: quantification of 6-NBDG uptake data, based on the geometric MFI, normalized to unstimulated Tconv cells (n=3), ****p=5.88x10^{-5}. Two-way ANOVA with Tukey's *post hoc* test was used for statistical analysis. Data are presented as mean ± SEM. Sample size (n) represents cells from individual donors, analyzed in independent experiments.

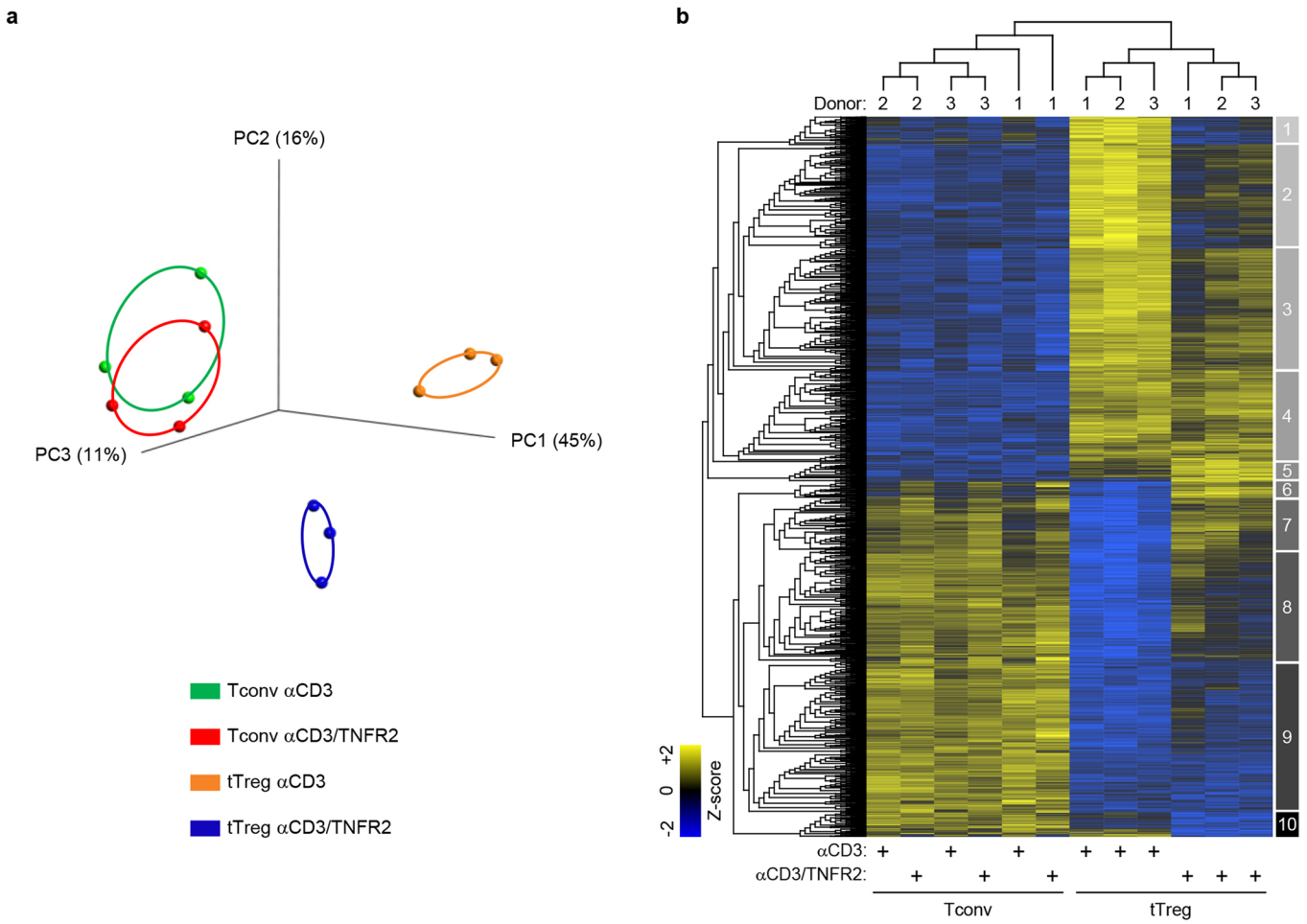

Extended Data Fig. 6 | Transcriptomic analysis of Tconv and tTreg cells upon TNFR2 costimulation. a, PCA plot of the transcriptomes of Tconv and tTreg cells that were activated via either CD3 or CD3/TNFR2 for 24 h (*n*=3 independent expansion cultures from different donors). **b**, Heat map showing hierarchical clustering of the 2664 genes that were differentially expressed between the comparative conditions. Z-scores showing relative gene expression values are color-coded. Grey-scale boxes (right) indicate clusters. Statistical evaluation was performed according to ANOVA with the Benjamini-Hochberg method with FDR<0.005.

Glycolysis/TCA cycle intermediates after αCD3 vs αCD3/TNFR2 in Tconv cells			
Metabolite	**Pathway/Process**	***p*-value***	**Log_2 fold change**
Dihydroxyacetone3P	Glycolysis	0.0141	0.8638
α-Ketoglutarate	TCA Cycle	0.0299	0.8492
Citrate	TCA Cycle	0.0369	0.3258

Glycolysis/TCA cycle intermediates after αCD3 vs αCD3/TNFR2 in tTreg cells			
Metabolite	**Pathway/Process**	***p*-value***	**Log_2 fold change**
Fructose16bisP	Glycolysis	0.0002	2.301
Glyceraldehyde3P	Glycolysis	0.0020	3.416
Dihydroxyacetone3P	Glycolysis	0.0037	2.508
2P-glycerate	Glycolysis	0.0468	0.967
SuccinylCoA	TCA Cycle	0.0122	1.941
Malate	TCA Cycle	0.0237	0.677
AcetylCoA	TCA Cycle	0.0239	0.973
Citrate	TCA Cycle	0.0298	0.360

Extended Data Fig. 7 | Significant changes in glycolysis/TCA cycle intermediates in Tconv and tTreg cells activated via CD3/TNFR2. Unpaired two-sided Student's *t*-test was used for statistical analysis (*). Data is derived from 4 independent expansion cultures of distinct donors.

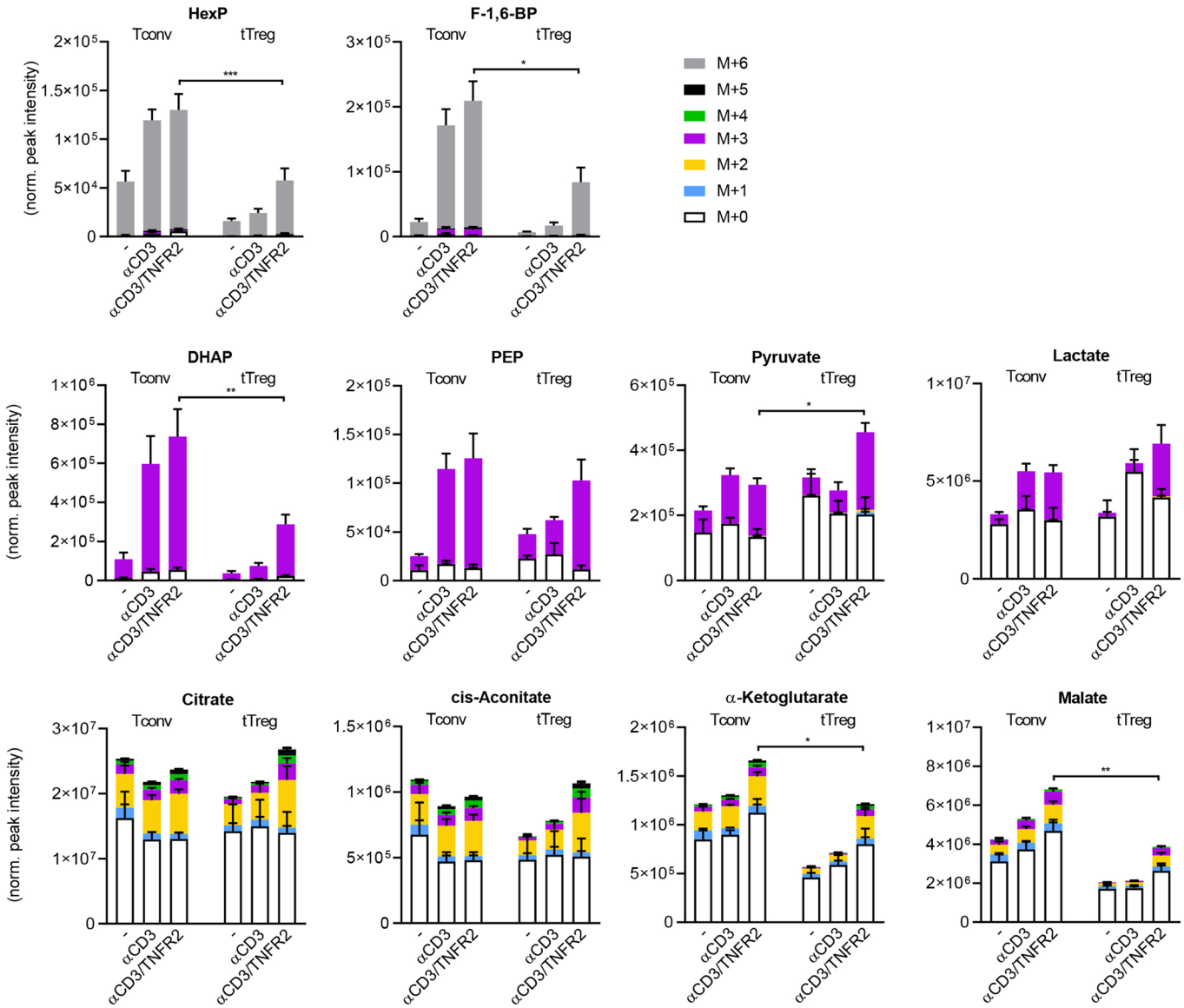

Extended Data Fig. 8 | Complete mass isotopologue analysis of glycolysis and TCA cycle intermediates upon [$^{13}C_6$]-glucose tracing in Tconv and tTreg cells. Levels of all detected mass isotopologues of the indicated metabolites in Tconv and tTreg cells that were unstimulated or activated via CD3 alone or CD3/TNFR2 for 24 h in the presence of [$^{13}C_6$]-glucose, as measured by LC-MS (n=4 independent expansion cultures, as in Fig. 5), ***p=0.0002 for HexP, *p=0.0381 for F-1,6-BP, **p=0.0029 for DHAP, *p=0.0397 for pyruvate, *p=0.0137 for α-ketoglutarate and **p=0.0029 for malate. Two-way ANOVA with Bonferroni's *post hoc* test was used for statistical analysis. Data are presented as mean ± SEM.

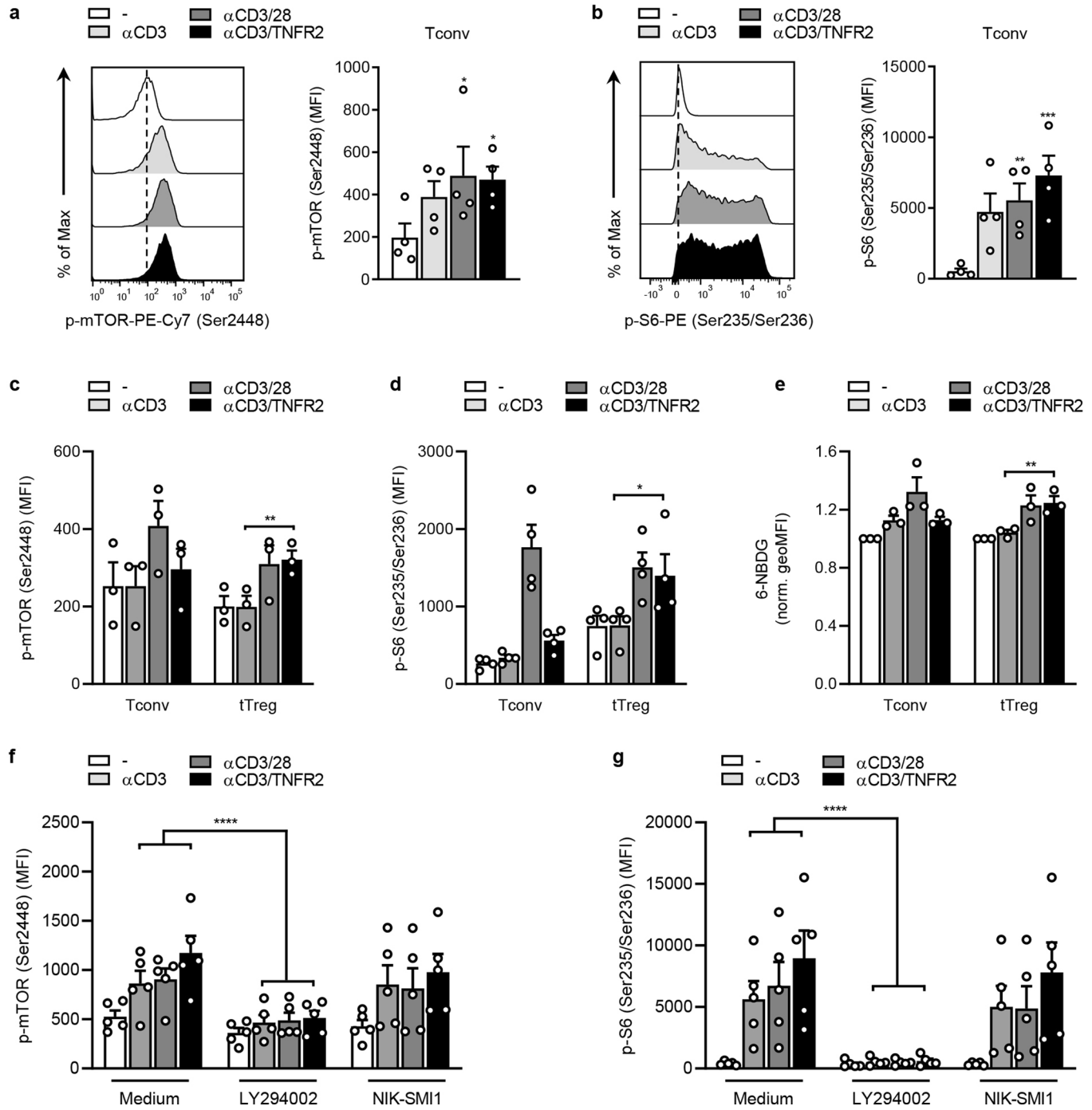

Extended Data Fig. 9 | Phosphorylation of mTOR and S6 in Tconv cells. a, Left panel: flow cytometric analysis of phosphorylated mTOR (Ser2448) levels in Tconv cells following stimulation for 24 h as indicated. Right panel: quantification based on MFI (n=4), *p=0.0131 and 0.0197 for αCD3/28 and αCD3/TNFR2 versus unstimulated, respectively. **b**, Left panel: flow cytometric analysis of phosphorylated S6 (Ser235/236) levels in Tconv cells following stimulation for 24 h as indicated. Right panel: quantification based on the MFI (n=4), **p=0.0026 and ***p=0.0003 for αCD3/28 and αCD3/TNFR2 versus unstimulated, respectively. (**a**, **b**) One-way repeated measures ANOVA with Bonferroni's *post hoc* test was used for statistical analysis. **c**, Quantification of phosphorylated mTOR (Ser2448) levels based on MFI in *ex vivo* naïve Tconv and tTreg cells stimulated for 24 h as indicated (n=3), **p=0.0039. **d**, Quantification of phosphorylated S6 (Ser235/236) levels based on MFI in *ex vivo* naïve Tconv and tTreg cells stimulated for 24 h as indicated (n=4), *p=0.0175. **e**, Quantification of 6-NBDG uptake activity in *ex vivo* naïve Tconv and tTreg cells stimulated for 24 h as indicated (n=3), **p=0.0015. **f**, **g**, Quantification of flow cytometric analysis of phosphorylated mTOR (Ser2448) (**f**) or S6 (Ser235/Ser236) (**g**) levels in Tconv cells following stimulation for 24 h as indicated in presence or absence of selective inhibitors of PI3K (LY294002) or NIK (NIK-SMI1) in the culture medium (n=5), ****p=4.54x10^{-6}, 2.13x10^{-6} and 5.2x10^{-10} for phosphorylated mTOR comparing medium versus LY294002 for αCD3, αCD3/28 and αCD3/TNFR2, respectively, and ****p=1.91x10^{-5}, 8.55x10^{-7} and 4.64x10^{-9} for phosphorylated S6 comparing medium versus LY294002 for αCD3, αCD3/28 and αCD3/TNFR2, respectively. (**c**–**g**) Two-way ANOVA with Tukey's *post hoc* test was used for statistical analysis. Data are presented as mean ± SEM. Sample size (n) represents cells from individual donors, analyzed in independent experiments.

nature research

Corresponding author(s): Jannie Borst

Last updated by author(s): Jul 7, 2020

Reporting Summary

Nature Research wishes to improve the reproducibility of the work that we publish. This form provides structure for consistency and transparency in reporting. For further information on Nature Research policies, see Authors & Referees and the Editorial Policy Checklist.

Statistics

For all statistical analyses, confirm that the following items are present in the figure legend, table legend, main text, or Methods section.

n/a	Confirmed
☐	☒ The exact sample size (*n*) for each experimental group/condition, given as a discrete number and unit of measurement
☐	☒ A statement on whether measurements were taken from distinct samples or whether the same sample was measured repeatedly
☐	☒ The statistical test(s) used AND whether they are one- or two-sided *Only common tests should be described solely by name; describe more complex techniques in the Methods section.*
☒	☐ A description of all covariates tested
☐	☒ A description of any assumptions or corrections, such as tests of normality and adjustment for multiple comparisons
☐	☒ A full description of the statistical parameters including central tendency (e.g. means) or other basic estimates (e.g. regression coefficient) AND variation (e.g. standard deviation) or associated estimates of uncertainty (e.g. confidence intervals)
☐	☒ For null hypothesis testing, the test statistic (e.g. *F*, *t*, *r*) with confidence intervals, effect sizes, degrees of freedom and *P* value noted *Give P values as exact values whenever suitable.*
☒	☐ For Bayesian analysis, information on the choice of priors and Markov chain Monte Carlo settings
☐	☒ For hierarchical and complex designs, identification of the appropriate level for tests and full reporting of outcomes
☐	☒ Estimates of effect sizes (e.g. Cohen's *d*, Pearson's *r*), indicating how they were calculated

Our web collection on statistics for biologists contains articles on many of the points above.

Software and code

Policy information about availability of computer code

Data collection	Flow cytometry data were acquired on a MoFlo Astrios (Becktman Coulter) with Summit software (v6.2) and on a BD FACS Aria II, BD LSR Fortessa or BD LSRII with BD FACSDIVA software (v8). RNA-seq data were collected on an Illumina HighSeq2500 sequencer. Metabolomics data were collected on an Exactive mass spectrometer and Sciex TripleTOF 6600. Real-time metabolic data were collected on a XFe24 analyzer. Quantitative PCR data were collected on a Roche LightCycler 480-II. Confocal microscopy images data were acquired on an Andor Dragonfly 505 spinning disk confocal adapted with a Leica DMi8 microscope.
Data analysis	RNA-seq data were analyzed with TopHat (v2.1.0), Bowtie 1, Itreecount (available through https://github.com/NKI-GCF/itreecount), Qlucore Omics Explorer (v3.4), R (v3.5.1), edgeR (v3.8.6), limma (v3.22.7) and Ingenuity Pathway Analysis (v52912811) software (available through https://digitalinsights.qiagen.com). GSEA software (v4.0.0) was used with the Hallmark gene sets listed in the Molecular Signatures Database (MSigDB) (v7.0) available through https://www.gsea-msigdb.org/gsea/index.jsp. Metabolomics data were analyzed using LCquan (v 2.9), PeakView (v2.2.0) and MultiQuant (v3.0.3) software. Real-time metabolic data were analyzed using Wave software (v2.6.0.31). Flow cytometric data were analyzed using FlowJo software (v10.5.3). Quantitative PCR data were analyzed using LightCycler 480 Software (v1.5). Image processing for confocal microscopy was performed using Fiji/ImageJ software (v1.52j) and colocalization was calculated using the JACoP plug-in. Statistical analyses were performed using GraphPad Prism (v8.1.1).

For manuscripts utilizing custom algorithms or software that are central to the research but not yet described in published literature, software must be made available to editors/reviewers. We strongly encourage code deposition in a community repository (e.g. GitHub). See the Nature Research guidelines for submitting code & software for further information.

Data

Policy information about availability of data

All manuscripts must include a data availability statement. This statement should provide the following information, where applicable:

- Accession codes, unique identifiers, or web links for publicly available datasets
- A list of figures that have associated raw data
- A description of any restrictions on data availability

RNA-seq data are deposited in the GEO database and available under accession code GSE138603 (https://www.ncbi.nlm.nih.gov/geo/query/acc.cgi?acc=GSE138603) and GSE138604 (https://www.ncbi.nlm.nih.gov/geo/query/acc.cgi?acc=GSE138604).
Gene set enrichment analysis was performed with GSEA software using the hallmark gene sets listed in the Molecular Signatures Database (MSigDB) available through https://www.gsea-msigdb.org/gsea/index.jsp.
The proteomics dataset used in this study is published by Cuadrado et al., Immunity, 2018 (DOI: 10.1016/j.immuni.2018.04.008).
All other data supporting the findings in this study are available from the corresponding author upon reasonable request.

Field-specific reporting

Please select the one below that is the best fit for your research. If you are not sure, read the appropriate sections before making your selection.

☒ Life sciences ☐ Behavioural & social sciences ☐ Ecological, evolutionary & environmental sciences

For a reference copy of the document with all sections, see nature.com/documents/nr-reporting-summary-flat.pdf

Life sciences study design

All studies must disclose on these points even when the disclosure is negative.

Sample size	No statistical analyses were performed to determine sample size. Sample sizes were chosen based on own previous experience and literature findings.
Data exclusions	Donors were excluded when expanded Treg cells contained >10% contaminated Tconv cells. Otherwise all data points were included in the analyses.
Replication	All analyses were done using at least 3 independent donors, processed in separate experiments at different time points. All attempts at replication are shown in the figures (derived from experiments performed at the Netherlands Cancer Institute and Leiden University Medical Center).
Randomization	No randomization has been done as all experiments involved a side-by-side comparison between Tconv and Treg cells in all conditions tested.
Blinding	Blinding was not relevant since analyses of the controls and experimental conditions were performed using the same gating strategies. In addition, Tconv and Treg cells from every single donor tested underwent the same experimental procedures in a side-by-side comparison.

Reporting for specific materials, systems and methods

We require information from authors about some types of materials, experimental systems and methods used in many studies. Here, indicate whether each material, system or method listed is relevant to your study. If you are not sure if a list item applies to your research, read the appropriate section before selecting a response.

Materials & experimental systems

n/a	Involved in the study
☐	☒ Antibodies
☒	☐ Eukaryotic cell lines
☒	☐ Palaeontology
☒	☐ Animals and other organisms
☐	☒ Human research participants
☒	☐ Clinical data

Methods

n/a	Involved in the study
☒	☐ ChIP-seq
☐	☒ Flow cytometry
☒	☐ MRI-based neuroimaging

Antibodies

Antibodies used	Following antibodies were used: CD3-FITC (BD Biosciences, clone: SK7; cat. no. 345763), 1:50 dilution CD3-PE (Dako, clone: UCHT1, cat. no. R0810), 1:50 dilution CD3-BV510 (BioLegend, clone: OKT3, cat. no. 317332), 1:50 dilution CD4-FITC (ImmunoTools, clone: OKT4, cat. no. 21850043X2), 1:50 dilution

CD4-PE-Cy7 (BioLegend, clone: OKT4, cat. no. 317414), 1:50 dilution
CD4-BB700 (BD Biosciences, clone: SK3, cat. no. 566392), 1:50 dilution
CD4-BV510 (BioLegend, clone: OKT4, cat. no. 317443), 1:50 dilution
CD8-APC (ImmunoTools, clone: HIT8a, cat. no. 21810086), 1:50 dilution
CD8-AlexaFluor700 (BioLegend, clone: SK1, cat. no. 344724), 1:50 dilution
CD19-BV510 (BioLegend, clone: HIB19, cat. no. 302242), 1:50 dilution
CD25-PE (BD Biosciences, clone: 2A3, cat. no. 341011), 1:20 dilution
CD28-PE-Cy5 (BioLegend, clone: CD28.2, cat. no. 302910), 1:50 dilution
CD45-PE-CF594 (BD Biosciences, clone: HI30, cat. no. 562279), 1:50 dilution
CD45RA-FITC (BioLegend, clone: HI100, cat. no. 304106), 1:50 dilution
CD45RA-APC-Cy7 (BioLegend, clone: HI100, cat. no. 304128), 1:50 dilution
CD45RA-BV650 (BD Biosciences, clone: HI100, cat.no. 304136), 1:50 dilution
CD69-PerCP-Cy5.5 (BioLegend, clone: FN50, cat. no. 310926), 1:50 dilution
CD127-BV421 (BioLegend, clone: A019D5, cat. no. 351310), 1:50 dilution
CD127-BV711 (BD Biosciences, clone: HIL-7R-M21, cat. no. 563165), 1:50 dilution
CD120b(TNFR2)-PE (Biolegend, clone: 3G7A02, cat. no. 358404), 1:50 dilution
CD120b(TNFR2)-PE-Cy7 (BioLegend, clone: 3G7A02, cat. no. 358412), 1:50 dilution
CD152(CTLA4)-PE-Dazzle594 (BioLegend, clone: L3D10, cat.no. 349922), 1:20 dilution
FOXP3-APC (Invitrogen, clone: PCH101, cat. no. 17-4776-42), 1:20 dilution
FOXP3-eFluor450 (Invitrogen, clone: PCH101, cat. no. 48-4776-42), 1:20 dilution
GLUT1 (Abcam, clone: EPR3915, cat. no. ab115730), 1:40 dilution
Anti-rabbit-AlexaFluor488 secondary Ab (Invitrogen, goat polyclonal Ab, A11008): 1:400 dilution
Helios(IKZF2)-PE-Cy7 (BioLegend, clone: 22F6, cat. no. 137236), 1:50 dilution
Helios(IKZF2)-PE-Dazzle594 (BioLegend, clone: 22F6, cat. no. 137232), 1:50 dilution
phospho-mTOR(Ser2448)-PE-Cy7 (Invitrogen, clone: MRRBY, cat.no. 25-9718-41), 1:50 dilution
phospho-S6(Ser235, Ser236)-PE (Invitrogen, clone: cupk43k, cat. no. 12-9007-41), 1:50 dilution

GPA33 antibody was provided by Prof. Andrew Scott to Dr. Amsen. Details regarding the antibody can be found in Herbertson et al., J Nucl Med, 2014. Antibody was conjugated in-house with Alexa Fluor 647 Succinimidyl Ester (Thermo Fisher Scientific) as used by Opstelten et al., JI, 2020. Antibody was used in a 1:1000 dilution.

CD3 (Sanquin, clone: CLB-T3/4.E, cat. no. M1654), 1:10,000 dilution
CD28 (Sanquin, clone: CLB-CD28/1, cat. no. M1650), 1:15,000 dilution
TNFR2 (Hycult Biotech, clone: MR2-1, cat. no. HM2007), 1:40 dilution

Validation

Antibodies are commercially available and have been validated by the manufacturer for intended application and have been extensively used in other peer-reviewed studies.

Human research participants

Policy information about studies involving human research participants

Population characteristics	The only donor information that is available is the gender (male). Donors are healthy volunteers aged 18-65.
Recruitment	We did not recruit donors, but made use of Sanquin's volunteer donor scheme.
Ethics oversight	Human materials were obtained in accordance with the Declaration of Helsinki and the Dutch rules with respect to the use of human materials from volunteer donors. Buffy coats from healthy anonymized male donors were obtained after their written informed consent, as approved by Sanquin's internal ethical board.

Note that full information on the approval of the study protocol must also be provided in the manuscript.

Flow Cytometry

Plots

Confirm that:

☒ The axis labels state the marker and fluorochrome used (e.g. CD4-FITC).

☒ The axis scales are clearly visible. Include numbers along axes only for bottom left plot of group (a 'group' is an analysis of identical markers).

☒ All plots are contour plots with outliers or pseudocolor plots.

☒ A numerical value for number of cells or percentage (with statistics) is provided.

Methodology

Sample preparation

PBMC were isolated by standard Ficoll density gradient centrifugation, followed by cell sorting and expansion as detailed in the materials and methods section. Following restimulation, cells were washed in PBS/1%FCS (FACS buffer) and surface stained for 20 min on ice. Following staining, cells were washed twice in FACS buffer. Fixation and permeabilization and subsequent washing steps were done using commercially available reagents as indicated in the materials and methods section. Cells were acquired in FACS buffer.

	For 6-NBDG uptake assays, cells were treated as indicated in the materials and methods section, and acquired in FACS buffer (while keeping the cells on ice until acquisition).
Instrument	MoFlo Astrios (Beckton Coulter) or BD FACS Aria II (BD Biosciences) for sorting, BD LSR Fortessa and BD LSRII for analysis.
Software	Summit (v6.2) for MoFlo Astrios, BD FACSDiva (v8) for acquisition on BD FACS Aria II, LSR Fortessa and LSRII, and FlowJo (v10.5.3) for analysis.
Cell population abundance	For cell sorting 500x10^6 PBMC were used (which yielded 50-100x10^6 CD4+ T cells) or whole buffy coat using the StraightFrom Buffy Coat CD4 microbead kit (Miltenyi) (which yielded 100-400x10^6 CD4+ T cells). Following sorting of ~100-150x10^6 CD4+ T cells, this generally yielded 2.5-10x10^6 naïve conventional T cells (~10-25% of total CD4+ T cells) and 100,000-350,000 naïve regulatory T cells (~0.5-1% of total CD4+ T cells). For sorting of effector conventional or regulatory T cells (GPA33low), we collected 1.5x10^6 effector conventional T cells. Effector Treg cells were subdivided into TNFR2low cells (0.5-1% of total CD4+ T cells) or TNFR2high cells (0.3-0.5% of total CD4+ T cells), yielding 250,000-400,000 TNFR2low and 75,000-150,000 TNFR2high effector Treg cells. After each sorting experiment, a purity check was done to confirm the purity of the samples.
Gating strategy	The gating strategy for sorting is detailed in Extended Data Figure 1 and Figure 8 of the manuscript. For analysis, cells were similarly gated: FSC-A/SSC-A, singlets (FSC-A/FSC-H) and live cells using a live/dead marker as detailed in the materials and methods section and in the Supplementary Information.

☒ Tick this box to confirm that a figure exemplifying the gating strategy is provided in the Supplementary Information.